Hindawi Publishing Corporation
Mathematical Problems in Engineering
Volume 2013, Article ID 491062, 19 pages
http://dx.doi.org/10.1155/2013/491062

Research Article

Torsional Vibrations of a Conic Shaft with Opposite Tapers Carrying Arbitrary Concentrated Elements

Jia-Jang Wu

Department of Marine Engineering, National Kaohsiung Marine University, No. 482, Jhong-Jhou 3rd Road, Cijin District, Kaohsiung City 80543, Taiwan

Correspondence should be addressed to Jia-Jang Wu; jjangwu@mail.nkmu.edu.tw

Received 20 December 2012; Accepted 3 February 2013

Academic Editor: Chang-Hua Lien

Copyright © 2013 Jia-Jang Wu. This is an open access article distributed under the Creative Commons Attribution License, which permits unrestricted use, distribution, and reproduction in any medium, provided the original work is properly cited.

The purpose of this paper is to present the exact solution for free torsional vibrations of a linearly tapered circular shaft carrying a number of concentrated elements. First of all, the equation of motion for free torsional vibration of a conic shaft is transformed into a Bessel equation, and, based on which, the exact displacement function in terms of Bessel functions is obtained. Next, the equations for compatibility of deformations and equilibrium of torsional moments at each attaching point (including the shaft ends) between the concentrated elements and the conic shaft with positive and negative tapers are derived. From the last equations, a characteristic equation of the form $[H]\{C\} = 0$ is obtained. Then, the natural frequencies of the torsional shaft are determined from the determinant equation $|H| = 0$, and, corresponding to each natural frequency, the column vector for the integration constants, $\{C\}$, is obtained from the equation $[H]\{C\} = 0$. Substitution of the last integration constants into the associated displacement functions gives the corresponding mode shape of the entire conic shaft. To confirm the reliability of the presented theory, all numerical results obtained from the exact method are compared with those obtained from the conventional finite element method (FEM) and good agreement is achieved.

1. Introduction

In this paper, a conic shaft with its longitudinal (lateral) surface generated by revolving an inclined straight line about its longitudinal axis is called the *general conic shaft* and that generated by revolving an inclined curve about its longitudinal axis is called the *specific conic shaft*. The main difference between the last two conic shafts is that the variation of cross-section area $A(x)$ is to take the form of $A(x) = A_\ell(x/L_\ell)^2$ for the general conic shaft and $A(x) = (ax + b)^n$ for the specific conic shaft. In the last expressions for $A(x)$, x denotes the longitudinal coordinate of the conic shaft with its origin at the tip (left) end of the general conic shaft, A_ℓ denotes the cross-sectional area at $x = L_\ell$ with the subscript ℓ denoting the larger end of the shaft, while a, b, and n denote constants (with $b \neq 0$). For a general conic shaft, the exact solution for the natural frequencies and mode shapes of free transverse vibrations has been presented in [1], while for a specific conic shaft, that of free longitudinal vibration has been reported in [2, 3], and that of free torsional vibration in [4]. However, for a general conic shaft, the information concerning its exact solution for the natural frequencies and mode shapes of free torsional vibration is not yet obtainable from the existing literature. In [2–4], the exact solution for free longitudinal or free torsional vibration of a specific conic rod is obtained by using appropriate transformations to reduce its equation of motion to the analytically solvable standard form with the specific area variation $A(x) = (a + bx)^n$. In [5], the numerical solution for the lowest several natural frequencies of the free-free specific conic shafts is determined from the so-called target function method. Because the exact solution for the natural frequencies and mode shapes of free torsional vibration of the most practical general conic shafts is not yet presented, this paper tries to provide some information for this topic.

For convenience, in this paper, a linearly tapered beam is called the *positive-taper* conic shaft if its cross-sectional diameter $d(x)$ increases with increasing the longitudinal coordinates x and is called the *negative-taper* conic shaft if its diameter $d(x)$ decreases with increasing x. Furthermore,

TABLE 1: The dimensions of a general conic shaft with five taper ratios $\overline{\alpha} = d_\ell/L_\ell$, larger-end diameter $d_\ell = 0.05$ m, and shaft length $L_{\text{shaft}} = L = 2.0$ m kept unchanged.

Case	Taper ratio $\overline{\alpha} = d_\ell/L_\ell$	Complete shaft length L_ℓ (m)	Length truncated L_s (m)	Smaller-end diameter d_s (m)	Shaft length $L_{\text{shaft}} = L$ (m)	Larger-end diameter d_ℓ (m)
1	0.02	2.5	0.5	0.01		
2	**0.01**	**5.0**	**3.0**	**0.03**		
3	0.005	10.0	8.0	0.04	2.0	0.05
4	0.0025	20.0	18.0	0.045		
5	0.001	50.0	48.0	0.048		
Uniform rod		—	—	0.05	2.0	0.05

a conic shaft consisting of one positive-taper conic shaft segment only is called the *P-taper* shaft (cf. Figures 1 and 2) and that composed of both a positive-taper and a negative-taper conic shaft segments is called the *PN-taper* shaft (cf. Figure 3). The exact natural frequencies and mode shapes for the free torsional vibrations of a P-taper shaft with or without carrying any number of concentrated elements (such as rigid disks and/or torsional springs) are determined through the following procedures: (a) to transform the equation of motion of the P-taper shaft into the Bessel equation and to obtain the exact solution for the (torsional) angular displacements in terms of the Bessel functions. (b) To establish the equations of compatibility for deformations and those of equilibrium for torsional moments at a typical intermediate node i connecting the conic shaft segments (i) and ($i + 1$), and those at the two ends of the entire conic shaft. Based on the last equations and the prescribed boundary conditions, corresponding to each of the trial natural frequencies, a characteristic equation for the entire conic shaft, $[H]\{C\} = 0$, is obtained, in which, $\{C\}$ is a column vector composed of the integration constants of all conic shaft segments and $[H]$ is a square matrix composed of the associated coefficients. (c) To determine the natural frequency of the vibrating system from the determinant equation $|H| = 0$ by using the bisectional method [6] and to obtain the associated integration constants from the equation $[H]\{C\} = 0$. The substitution of the latter integration constants into the associated displacement function for each of the conic shaft segments will determine the corresponding mode shape. The last steps (b) and (c) must be repeated q cycles if q pairs of natural frequency and associated mode shape are required. It is found that the foregoing procedures for obtaining the exact solution of free torsional vibrations of a P-taper shaft are also available for that of a PN-taper shaft carrying arbitrary concentrated elements. The key point is to replace the longitudinal (axial) coordinate x for the positive-taper part of the PN-taper shaft by $\overline{x} = L_\ell + \overline{L}_\ell - x$ for the negative-taper part of the PN-taper shaft (cf. Figure 3) and the parameters (d_s, d_ℓ, L_s, and L_ℓ) for the positive-taper part by those ($\overline{d}_s$, $\overline{d}_\ell$, $\overline{L}_s$, and $\overline{L}_\ell$) for the negative-taper part, where d_s and d_ℓ denote the diameters at smaller and larger ends of the positive-taper part, $\overline{d}_s$ and $\overline{d}_\ell$ denote the corresponding ones of the negative-taper part, L_s and L_ℓ denote the coordinates of smaller and larger ends of the positive-taper part with origin o at the tip of the complete positive-taper cone, while $\overline{L}_s$ and $\overline{L}_\ell$ denote those of the negative-taper part with origin $\overline{o}$ at the tip of the complete negative-taper cone (cf. Figure 3).

To confirm the reliability of the presented exact method, the influence of taper ratios ($\overline{\alpha}$) of the P-taper and PN-taper shafts on their lowest four natural frequencies in various boundary conditions (BCs) is studied. It is found that the lowest four natural frequencies of all conic shafts converge to the corresponding ones of the associated uniform shafts in various BCs when the taper ratios of the conic shafts approach zero (i.e., $\overline{\alpha} \approx 0$). Furthermore, all numerical results obtained from the presented exact method are also compared with those obtained from the conventional finite element method (FEM) and good agreement is achieved. For convenience, a conic shaft without any attachments is called the *bare shaft* and the one carrying any concentrated elements is called the *loaded shaft* in this paper.

2. Bessel Equation for the Torsional Vibration of a P-Taper Conic Shaft

For a nonuniform shaft performing free torsional vibrations, its equation of motion takes the form [7]:

$$\frac{\partial}{\partial x}\left[GI_P(x)\frac{\partial\theta(x,t)}{\partial x}\right] = \rho I_P(x)\frac{\partial^2\theta(x,t)}{\partial t^2}, \qquad (1)$$

where ρ and G are mass density and shear modulus of the shaft material, respectively, $I_p(x)$ is the polar moment of inertia for the cross-sectional area $A(x)$ of the shaft at position x, and $\theta(x,t)$ is the torsional angle of the shaft at position x and time t. For the P-taper conic shaft as shown in Figure 1, x is the axial coordinate with its origin o at the tip end of the complete conic shaft. It is evident that the revolution of the inclined straight line $\overline{AB}$ about the horizontal x-axis will generate the longitudinal (lateral) surface of the shaft.

If d_ℓ denotes the diameter of the larger end of the truncated conic shaft (cf. Figure 1), then the diameter for the cross-section area located at position x is given by

$$d_x = \left(\frac{x}{L_\ell}\right)d_\ell, \qquad (2)$$

TABLE 2: Influence of taper ratio ($\overline{\alpha} = d_\ell / L_\ell$) on the lowest five natural frequencies ω_τ (rad/sec) of the P-taper conic shaft (cf. Figure 5) with larger-end diameter $d_\ell = 0.05$ m and shaft length $L_{\text{shaft}} = L = 2.0$ m kept unchanged: (a) F-F, (b) C-C, (c) C-F, and (d) F-C BCs.

(a)

Case	Taper ratios $\overline{\alpha}$	Method	Natural frequencies, ω_τ (rad/sec)				
			ω_1	ω_2	ω_3	ω_4	ω_5
1	0.02	Exact#	7384.4129	11854.5424	16427.4469	21133.5082	25931.2855
		FEM*	7382.5338	11854.2819	16438.2035	21170.1886	26013.7379
2	0.01	Exact	5374.8958	10198.6873	15134.0131	20100.9780	25081.0046
		FEM	5375.3828	10204.5966	15155.2176	20152.2975	25182.2201
3	0.005	Exact	5074.8956	10037.9356	15025.4133	20019.1472	25015.3982
		FEM	5075.6554	10044.3910	15047.4403	20071.5715	25118.0086
4	0.0025	Exact	5016.8720	10008.5200	15005.7524	20004.3882	25003.5861
		FEM	5017.6806	10015.0732	15027.9268	20057.0107	25106.4467
5	0.001	Exact	5002.5736	10001.3500	15000.9698	20000.8006	25000.7158
		FEM	5003.3940	10007.9269	15023.1800	20053.4711	25103.6372
	Uniform shaft**		**5000.0416**	**10000.0832**	**15000.1248**	**20000.1664**	**25000.2080**

#Natural frequencies obtained from presented exact method using single shaft segment ($P = 1$).
*Natural frequencies obtained from finite element method using 50 shaft elements ($n_e = 50$).
**The exact natural frequencies of uniform shaft obtained from formulas in the appendix.

(b)

Case	Taper ratios $\overline{\alpha}$	Method	Natural frequencies, ω_τ (rad/sec)				
			ω_1	ω_2	ω_3	ω_4	ω_5
1	0.02	Exact#	5966.9661	10667.3679	15490.2119	20382.6984	25312.3748
		FEM*	5966.2987	10670.9583	15508.0439	20429.6221	25408.1553
2	0.01	Exact	5128.1859	10066.7014	15044.8782	20033.8229	25027.1676
		FEM	5128.8914	10073.0559	15066.7556	20086.0475	25129.5265
3	0.005	Exact	5025.1181	10012.7167	15008.5594	20006.4959	25005.2732
		FEM	5025.9195	10019.2558	15030.7127	20059.0900	25108.0980
4	0.0025	Exact	5005.6582	10002.8966	15002.0014	20001.5744	25001.3349
		FEM	5006.4761	10009.4684	15024.2039	20054.2346	25104.2431
5	0.001	Exact	5005.6582	10002.8966	15002.0014	20001.5744	25001.3349
		FEM	5001.7077	10007.0855	15022.6214	20053.0546	25103.3066
	Uniform shaft**		**5000.0416**	**10000.0832**	**15000.1248**	**20000.1664**	**25000.2080**

(c)

Case	Taper ratios $\overline{\alpha}$	Method	Natural frequencies, ω_τ (rad/sec)				
			ω_1	ω_2	ω_3	ω_4	ω_5
1	0.02	Exact#	447.0176	7811.0650	12760.2959	17706.1543	22667.7637
		FEM*	447.9340	7812.6640	12771.1535	17738.7421	22739.4090
2	0.01	Exact	1579.8439	7313.7896	12390.7453	17422.4856	22439.9285
		FEM	1580.1051	7316.8955	12404.1570	17458.5569	22515.9715
3	0.005	Exact	2068.4024	7379.8464	12428.7547	17449.3316	22460.7130
		FEM	2068.5822	7382.8417	12441.9769	17485.1338	22536.4057
4	0.0025	Exact	2290.9387	7435.7082	12461.7079	17472.7621	22478.9027
		FEM	2291.0813	7438.6027	12474.7612	17508.3261	22554.2862
5	0.001	Exact	2417.9471	7473.5121	12484.2105	17488.8006	22491.3660
		FEM	2418.0663	7476.3373	12497.1478	17524.2010	22566.5373
	Uniform shaft**		**2500.0208**	**7500.0624**	**12500.1040**	**17500.1456**	**22500.1872**

(d)

Case	Taper ratios $\overline{\alpha}$	Method	Natural frequencies, ω_τ (rad/sec)				
			ω_1	ω_2	ω_3	ω_4	ω_5
1	0.02	Exact#	5735.5766	9980.7807	14380.7452	18967.7823	23687.7230
		FEM*	5733.4631	9977.5119	14382.5800	18986.8702	23741.3914
2	0.01	Exact	3610.0689	8006.2117	12816.3662	17728.7711	22678.9066
		FEM	3609.7962	8007.9786	12827.5397	17761.6872	22750.8551

(d) Continued.

Case	Taper ratios $\overline{\alpha}$	Method	Natural frequencies, ω_τ (rad/sec)				
			ω_1	ω_2	ω_3	ω_4	ω_5
3	0.005	Exact	2969.4822	7681.4675	12610.5906	17579.4008	22561.9393
		FEM	2969.4664	7683.8987	12622.8685	17613.8717	22635.9044
4	0.0025	Exact	2717.6065	7578.0625	12547.2117	17533.8559	22526.4265
		FEM	2717.6603	7580.6924	12559.8220	17568.7953	22600.9996
5	0.001	Exact	2583.3737	7528.6619	12517.3057	17512.4412	22509.7535
		FEM	2583.4588	7531.3848	12530.0716	17547.6000	22584.6113
Uniform shaft**			**2500.0208**	**7500.0624**	**12500.1040**	**17500.1456**	**22500.1872**

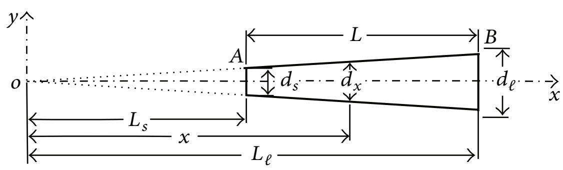

Figure 1: The coordinate system for a P-taper conic shaft with diameter d_ℓ at its larger end, diameter d_s at its smaller end, and length $L_{\text{shaft}} = L = L_\ell - L_s$.

where L_ℓ is the total length of the complete conic shaft, and the polar moment of inertia $I_p(x)$ of the cross-sectional area is given by

$$I_p(x) = \frac{\pi d_x^4}{32} = \left(\frac{x}{L_\ell}\right)^4 I_{p,\ell}, \tag{3}$$

where $I_{p,\ell}$ is the polar moment of inertia for the cross-sectional area at larger end of the conic shaft given by

$$I_{p,\ell} = \frac{\pi d_\ell^4}{32}. \tag{4}$$

For free vibrations, one has

$$\theta(x,t) = \Theta(x)\, e^{j\omega t}, \tag{5}$$

where $\Theta(x)$ denotes the amplitude of $\theta(x,t)$, and ω denotes the angular natural frequency of conic shaft and $j = \sqrt{-1}$.

Substitution of (3) and (5) into (1) gives

$$\frac{d}{dx}\left[x^4 \frac{d\Theta(x)}{dx}\right] + \beta^2 x^4 \Theta(x) = 0, \tag{6}$$

where

$$\beta^2 = \frac{\rho\omega^2}{G}. \tag{7}$$

Equation (6) is a Bessel equation with its solution composed of the Bessel functions.

3. Displacement Function for the Conic Shaft

From [8–10], it can be found that the solution for the next differential equation:

$$\frac{d}{d\chi}\left[\chi^m \frac{dy}{d\chi}\right] + c\chi^n y = 0 \tag{8}$$

is given by

$$y = \chi^{\nu/\alpha}\left[C_1 J_\nu(z) + C_2 Y_\nu(z)\right], \tag{9}$$

where $J_\nu(z)$ and $Y_\nu(z)$ are 1st and 2nd kind Bessel functions of order ν, and the other parameters are given by

$$\alpha = \frac{2}{n-m+2}, \tag{10a}$$

$$\nu = \frac{1-m}{n-m+2}, \tag{10b}$$

$$z = \chi^{1/\alpha}\alpha\sqrt{c}. \tag{10c}$$

Comparing (8) with (6), one finds that

$$\chi = x, \qquad y = \Theta, \qquad m = 4, \qquad n = 4, \qquad c = \beta^2. \tag{11}$$

Substituting (11) into (10a), (10b), and (10c), one obtains,

$$\alpha = 1, \tag{12a}$$

$$\nu = -\frac{3}{2}, \tag{12b}$$

$$z = \chi^{1/\alpha}\alpha\sqrt{c} = x\beta. \tag{13}$$

Substituting the last parameters into (9) and using the relationship $Y_{\nu/2}(z) \propto J_{-\nu/2}(z)$ [8], one has

$$\Theta_\tau(z_\tau) = \beta_\tau^{3/2} z_\tau^{-3/2}\left[C_1^{(\tau)} J_{3/2}(z_\tau) + C_2^{(\tau)} J_{-3/2}(z_\tau)\right], \tag{14}$$

where

$$z_\tau = \beta_\tau x, \tag{15a}$$

$$\beta_\tau^2 = \frac{\rho\omega_\tau^2}{G}. \tag{15b}$$

In (14), (15a), and (15b), the subscript (or superscript) τ refers to the τth vibrating mode of the conic shaft, while $C_1^{(\tau)}$ and $C_2^{(\tau)}$ denote the two corresponding integration constants determined by the associated boundary conditions of the entire conic shaft.

Table 3: Influence of taper ratio ($\overline{\alpha} = d_\ell / L_\ell$) on the lowest five natural frequencies ω_τ (rad/sec) of the PN-taper shaft $\overline{ABC}$ (cf. Figure 3 or Figure 4(a)) with dimensions of its negative-taper part $\overline{BC}$ identical to the corresponding ones of its positive-taper part $\overline{AB}$, and the larger-end diameter $d_\ell = 0.05$ m and total shaft length $L_{\text{shaft}} = L = 4.0$ m kept unchanged: (a) F-F, (b) C-C, and (c) C-F (or F-C) BCs.

(a)

Case	Taper ratios $\overline{\alpha}$	Method	Natural frequencies, ω_τ (rad/sec)				
			ω_1	ω_2	ω_3	ω_4	ω_5
1	0.02	Exact#	5735.5766	7384.4129	9980.7807	11854.5424	14380.7452
		FEM*	5733.4631	7382.5338	9977.5119	11854.2819	14382.5800
2	0.01	Exact	3610.0689	5374.8958	8006.2117	10198.6873	12816.3662
		FEM	3609.7962	5375.3828	8007.9786	10204.5966	12827.5397
3	0.005	Exact	2969.4822	5074.8956	7681.4675	10037.9356	12610.5906
		FEM	2969.4664	5075.6554	7683.8987	10044.3910	12622.8685
4	0.0025	Exact	2717.6065	5016.8720	7578.0625	10008.5200	12547.2117
		FEM	2717.6603	5017.6806	7580.6924	10015.0732	12559.8220
5	0.001	Exact	2583.3737	5002.5736	7528.6619	10001.3500	12517.3057
		FEM	2583.4588	5003.3940	7531.3848	10007.9269	12530.0716
	Uniform shaft**		**2500.0208**	**5000.0416**	**7500.0624**	**10000.0832**	**12500.1040**

#Natural frequencies obtained from presented exact method using two shaft segments ($P = 2$).
*Natural frequencies obtained from finite element method using 100 shaft elements ($n_e = 100$).
**The exact natural frequencies of uniform shaft obtained from formulas in the appendix.

(b)

Case	Taper ratios $\overline{\alpha}$	Method	Natural frequencies, ω_τ (rad/sec)				
			ω_1	ω_2	ω_3	ω_4	ω_5
1	0.02	Exact#	447.0176	5966.9661	7811.0650	10667.3679	12760.2959
		FEM*	447.9340	5966.2987	7812.6640	10670.9583	12771.1535
2	0.01	Exact	1579.8439	5128.1859	7313.7896	10066.7014	12390.7453
		FEM	1580.1051	5128.8914	7316.8955	10073.0559	12404.1570
3	0.005	Exact	2068.4024	5025.1181	7379.8464	10012.7167	12428.7547
		FEM	2068.5822	5025.9195	7382.8417	10019.2558	12441.9769
4	0.0025	Exact	2290.9387	5005.6582	7435.7082	10002.8966	12461.7079
		FEM	2291.0813	5006.4761	7438.6027	10009.4684	12474.7612
5	0.001	Exact	2417.9471	5000.8859	7473.5121	10000.5058	12484.2105
		FEM	2418.0663	5001.7077	7476.3373	10007.0855	12497.1478
	Uniform shaft**		**2500.0208**	**5000.0416**	**7500.0624**	**10000.0832**	**12500.1040**

(c)

Case	Taper ratios $\overline{\alpha}$	Method	Natural frequencies, ω_τ (rad/sec)				
			ω_1	ω_2	ω_3	ω_4	ω_5
1	0.02	Exact#	314.6200	5841.7915	7596.9631	10286.6906	12314.5569
		FEM*	315.2569	5840.2785	7596.7480	10286.1690	12319.6401
2	0.01	Exact	1016.5493	4182.8341	6408.1802	8927.6668	11352.3196
		FEM	1016.6576	4182.8740	6409.6737	8931.5092	11361.3636
3	0.005	Exact	1197.3804	3842.8258	6280.1632	8784.1136	11269.3945
		FEM	1197.4156	3843.1091	6281.7514	8788.4149	11278.7052
4	0.0025	Exact	1237.8483	3771.2365	6256.7605	8757.6678	11254.3883
		FEM	1237.8664	3771.5690	6258.3630	8762.0525	11263.7458
5	0.001	Exact	1248.1680	3753.2346	6251.0591	8751.2135	11250.7384
		FEM	1248.1817	3753.5794	6252.6651	8755.6185	11260.1073
	Uniform shaft**		**1250.0104**	**3750.0312**	**6250.0520**	**8750.0728**	**11250.0936**

TABLE 4: Influence of rigid disks (each with rotary inertia $\hat{J}_i = J^*/3$) or/and torsional springs (each with stiffness $\hat{k}_{t,i} = k_t^*/3$) on the lowest five natural frequencies of the P-taper conic shaft (cf. Figures 6 and case 2 of Table 1) with reference polar mass moment of inertia $J^* = 5.4409436902 \times 10^{-3}$ kg-m^2 and reference torsional stiffness $k_t^* = 1.378230198 \times 10^4$ Nm/rad.

Case	$N_{\hat{J}}$	$N_{\hat{k}_t}$	$\hat{J}_i$	$\hat{k}_{t,i}$	Method	Natural frequencies, ω_τ (rad/sec) $\omega_0^{\#}$	ω_1	ω_2	ω_3	ω_4
1	3	0	$\frac{1}{3}J^*$	0	Exact	—	2475.3743	5026.7728	10924.0242	12894.1665
					FEM	—	2475.4996	5027.4548	10931.3000	12904.4532
2	0	3	0	$\frac{1}{3}k_t^*$	Exact	1684.6341	5932.6585	10654.8699	15394.2260	20355.8291
					FEM	1684.7292	5933.5926	10661.9274	15416.7018	20409.3205
3	3	3	$\frac{1}{3}J^*$	$\frac{1}{3}k_t^*$	Exact	1168.6767	2853.7625	5191.2778	10939.0990	12923.7224
					FEM	1168.6972	2853.8492	5191.9785	10946.3775	12934.0271
	Bare F-F P-taper shaft*				Exact	—	**5374.8958**	**10198.6873**	**15134.0131**	**20100.9780**

*The exact values for the lowest four natural frequencies of the "bare" free-free P-taper shaft taken from case 2 of Table 2(a).
#Natural frequencies of quasi rigid-body modes.

TABLE 5: Influence of rigid disks (each with rotary inertia $\hat{J}_i = J^*/5$) or/and torsional springs (each with stiffness $\hat{k}_{t,i} = k_t^*/5$) on the lowest five natural frequencies of the free-free PN-taper conic shaft (cf. Figure 8 and case 2 of Table 1) with reference polar mass moment of inertia $J^* = 1.0881887380 \times 10^{-2}$ kg-m^{2}and reference stiffness of torsional springs $k_t^* = 6.891150988 \times 10^3$ N-m/rad.

Case	$N_{\hat{J}}$	$N_{\hat{k}_t}$	$\hat{J}_i$	$\hat{k}_{t,i}$	Method	Natural frequencies, ω_τ (rad/sec) $\omega_0^{\#}$	ω_1	ω_2	ω_3	ω_4
1	5	0	$\frac{1}{5}J^*$	0	Exact	—	1688.3916	2388.5998	3733.3469	5098.3850
					FEM	—	1688.3959	2388.7487	3733.5282	5099.2798
2	0	5	0	$\frac{1}{5}k_t^*$	Exact	862.2360	3832.1008	5552.7121	8137.9636	10337.4211
					FEM	862.2638	3831.8884	5553.3272	8139.9447	10343.6571
3	5	5	$\frac{1}{5}J^*$	$\frac{1}{5}k_t^*$	Exact	587.7894	1836.1973	2489.3670	3791.2496	5136.1437
					FEM	587.7957	1836.1865	2489.5046	3791.4298	5137.0417
	Bare F-F PN-taper shaft*				Exact	—	**3610.0689**	**5374.8958**	**8006.2117**	**10198.6873**

*The exact values for the lowest four natural frequencies of the "bare" free-free PN-taper shaft taken from case 2 of Table 3(a).
#Natural frequencies of quasi rigid-body modes.

4. Boundary Conditions

Figure 2 shows a free-free P-taper conic shaft composed of p conic shaft segments (denoted by $(1), (2), \ldots, (i), \ldots, (p)$) and carrying one rigid disk with polar mass moment of inertia $\hat{J}_i$ and one torsional spring with stiffness $\hat{k}_{t,i}$ at each node i ($i = 0, 1, 2, \ldots, p$). The compatibility of twisting angles and equilibrium of torques at the arbitrary intermediate node i located at $x = x_i$ require that

$$\Theta_{\tau,i}(z_{\tau,i}) = \Theta_{\tau,i+1}(z_{\tau,i}), \tag{16a}$$

$$GI_{p,i}\Theta'_{\tau,i}(z_{\tau,i}) = GI_{p,i}\Theta'_{\tau,i+1}(z_{\tau,i}) + \left(\omega_\tau^2 \hat{J}_i - \hat{k}_{t,i}\right)\Theta_{\tau,i}(z_{\tau,i}), \tag{16b}$$

where

$$z_{\tau,i} = \beta_\tau x_i, \tag{17a}$$

$$I_{p,i} = \left(\frac{x_i}{L_\ell}\right)^4 I_{p,\ell}. \tag{17b}$$

The boundary condition for the left end of the entire conic shaft is given by

$$GI_{p,0}\Theta'_{\tau,1}(z_{\tau,0}) + \left(\omega_\tau^2 \hat{J}_0 - \hat{k}_{t,0}\right)\Theta_{\tau,1}(z_{\tau,0}) = 0, \tag{18}$$

where

$$z_{\tau,0} = \beta_\tau x_0 = \beta_\tau L_s, \tag{19a}$$

$$I_{p,0} = \left(\frac{x_0}{L_\ell}\right)^4 I_{p,\ell} = \left(\frac{L_s}{L_\ell}\right)^4 I_{p,\ell}. \tag{19b}$$

Similarly, the boundary condition for the right end of the entire conic shaft is

$$GI_{p,p}\Theta'_{\tau,p}(z_{\tau,p}) - \left(\omega_\tau^2 \hat{J}_p - \hat{k}_{t,p}\right)\Theta_{\tau,p}(z_{\tau,p}) = 0, \tag{20}$$

where

$$z_{\tau,p} = \beta_\tau x_p = \beta_\tau L_\ell, \tag{21a}$$

$$I_{p,p} = \left(\frac{x_p}{L_\ell}\right)^4 I_{p,\ell} = \left(\frac{L_\ell}{L_\ell}\right)^4 I_{p,\ell} = I_{p,\ell}. \tag{21b}$$

Equations (18) and (20) are the nonclassical boundary conditions. The general classical boundary conditions (without any attachments at each end of the shaft) are given by

$$\Theta'_{\tau,1}(z_{\tau,0}) = 0, \tag{22a}$$

$$\Theta'_{\tau,p}(z_{\tau,0}) = 0 \quad (\text{for F-F shaft}), \tag{22b}$$

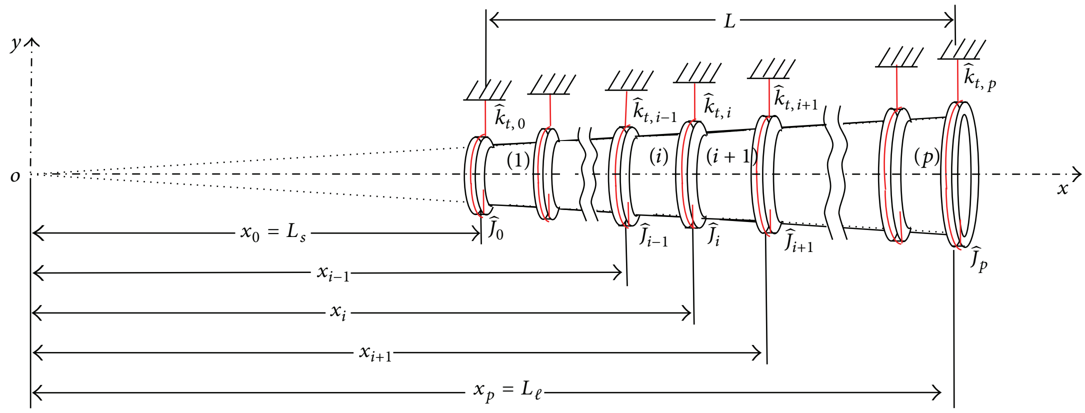

FIGURE 2: A free-free P-taper conic shaft composed of p conic shaft segments (denoted by $(1), (2), \ldots, (i), \ldots, (p)$) and carrying one rigid disk with polar mass moment of inertia $\hat{J}_i$ and one torsional spring with stiffness $\hat{k}_{t,i}$ at each node i ($i = 0, 1, 2, \ldots, p$).

$$\Theta_{\tau,1}(z_{\tau,0}) = 0, \tag{23a}$$

$$\Theta_{\tau,p}(z_{\tau,0}) = 0 \quad (\text{for C-C shaft}), \tag{23b}$$

$$\Theta_{\tau,1}(z_{\tau,0}) = 0, \tag{24a}$$

$$\Theta'_{\tau,p}(z_{\tau,0}) = 0 \quad (\text{for C-F shaft}), \tag{24b}$$

$$\Theta'_{\tau,1}(z_{\tau,0}) = 0, \tag{25a}$$

$$\Theta_{\tau,p}(z_{\tau,0}) = 0 \quad (\text{for F-C shaft}). \tag{25b}$$

In (22a)–(25b), the capital letters F and C denote the free and clamped ends of the entire shaft, respectively. Besides, the symbols $\Theta_{\tau,1}(z_{\tau,0})$ and $\Theta'_{\tau,1}(z_{\tau,0})$ denote the twisting angle and its first derivative of the first shaft segment at (left end) node o (cf. Figure 2), respectively. Similarly, $\Theta_{\tau,p}(z_{\tau,p})$ and $\Theta'_{\tau,p}(z_{\tau,p})$ denote those of the final (pth) shaft segment at (right end) node p, respectively.

5. Determination of Exact Natural Frequencies and Mode Shapes

From (14), the displacement function of the ith conic shaft segment takes the form

$$\Theta_{\tau,i}(z_{\tau,i}) = \beta_\tau^{3/2} z_{\tau,i}^{-3/2}\left[C_{1,i}^{(\tau)} J_{3/2}(z_{\tau,i}) + C_{2,i}^{(\tau)} J_{-3/2}(z_{\tau,i})\right]. \tag{26a}$$

Therefore,

$$\begin{aligned}\Theta'_{\tau,i}(z_{\tau,i}) &= \frac{d\Theta_{\tau,i}(z_{\tau,i})}{dx} \\ &= \beta_\tau^{5/2} z_{\tau,i}^{-3/2}\left\{-\frac{3}{2} z_{\tau,i}^{-1}\left[C_{1,i}^{(\tau)} J_{3/2}(z_{\tau,i}) + C_{2,i}^{(\tau)} J_{-3/2}(z_{\tau,i})\right]\right. \\ &\quad \left. + \left[C_{1,i}^{(\tau)} J'_{3/2}(z_{\tau,i}) + C_{2,i}^{(\tau)} J'_{-3/2}(z_{\tau,i})\right]\right\},\end{aligned} \tag{26b}$$

in which [11]

$$J_{3/2}(z) = \left(\frac{2}{\pi z}\right)^{1/2}\left(-\cos z + \frac{\sin z}{z}\right), \tag{27}$$

$$J_{-3/2}(z) = \left(\frac{2}{\pi z}\right)^{1/2}\left(-\sin z - \frac{\cos z}{z}\right), \tag{28}$$

$$J'_\nu(z) = \frac{dJ_\nu}{dz} \quad \left(\nu = \frac{3}{2} \text{ or } \frac{-3}{2}\right). \tag{29}$$

Now, the exact natural frequencies and the associated mode shapes of a conic shaft carrying arbitrary number of concentrated elements (including rigid disks and/or torsional springs) with various boundary conditions can be determined as follows.

5.1. Free-Free P-Taper Conic Shaft. For the free-free P-taper conic shaft shown in Figure 2, the substitutions of (26a) and (26b) into (18) lead to

$$\begin{aligned}&C_{1,1}^{(\tau)}\left\{\left[-\frac{3}{2}\beta_\tau z_{\tau,0}^{-1} + f_{\tau,0}\right] J_{3/2}(z_{\tau,0}) + \beta_\tau J'_{3/2}(z_{\tau,0})\right\} \\ &\quad + C_{2,1}^{(\tau)}\left\{\left[-\frac{3}{2}\beta_\tau z_{\tau,0}^{-1} + f_{\tau,0}\right] J_{-3/2}(z_{\tau,0}) + \beta_\tau J'_{-3/2}(z_{\tau,0})\right\} = 0,\end{aligned} \tag{30}$$

where

$$f_{\tau,0} = \frac{\left(\omega_\tau^2 \hat{J}_0 - \hat{k}_{t,0}\right)}{\left(GI_{p,0}\right)}. \tag{31}$$

Similarly, substituting (26a) and (26b) into (16a) and (16b), respectively, one obtains

$$C_{1,i}^{(\tau)} J_{3/2}(z_{\tau,i}) + C_{2,i}^{(\tau)} J_{-3/2}(z_{\tau,i}) - C_{1,i+1}^{(\tau)} J_{3/2}(z_{\tau,i}) - C_{2,i+1}^{(\tau)} J_{-3/2}(z_{\tau,i}) = 0, \tag{32}$$

$$\begin{aligned} &C_{1,i}^{(\tau)} \left\{ \left[-\frac{3}{2}\beta_\tau z_{\tau,i}^{-1} - f_{\tau,i} \right] J_{3/2}(z_{\tau,i}) + \beta_\tau J'_{3/2}(z_{\tau,i}) \right\} \\ &+ C_{2,i}^{(\tau)} \left\{ \left[-\frac{3}{2}\beta_\tau z_{\tau,i}^{-1} - f_{\tau,i} \right] J_{-3/2}(z_{\tau,i}) + \beta_\tau J'_{-3/2}(z_{\tau,i}) \right\} \\ &+ C_{1,i+1}^{(\tau)} \beta_\tau \left[\frac{3}{2} z_{\tau,i}^{-1} J_{3/2}(z_{\tau,i}) - J'_{3/2}(z_{\tau,i}) \right] \\ &+ C_{2,i+1}^{(\tau)} \beta_\tau \left[\frac{3}{2} z_{\tau,i}^{-1} J_{-3/2}(z_{\tau,i}) - J'_{-3/2}(z_{\tau,i}) \right] = 0, \end{aligned} \tag{33}$$

where

$$f_{\tau,i} = \frac{\left(\omega_\tau^2 \widehat{J}_i - \widehat{k}_{t,i}\right)}{\left(GI_{p,i}\right)}. \tag{34}$$

Finally, the substitution of (26a) and (26b) into (20) leads to

$$\begin{aligned} &C_{1,p}^{(\tau)} \left\{ \left[-\frac{3}{2}\beta_\tau z_{\tau,p}^{-1} - f_{\tau,p} \right] J_{3/2}(z_{\tau,p}) + \beta_\tau J'_{3/2}(z_{\tau,p}) \right\} \\ &+ C_{2,p}^{(\tau)} \left\{ \left[-\frac{3}{2}\beta_\tau z_{\tau,p}^{-1} - f_{\tau,p} \right] J_{-3/2}(z_{\tau,p}) + \beta_\tau J'_{-3/2}(z_{\tau,p}) \right\} = 0, \end{aligned} \tag{35}$$

where

$$f_{\tau,p} = \frac{\left(\omega_\tau^2 \widehat{J}_p - \widehat{k}_{t,p}\right)}{\left(GI_{p,p}\right)}. \tag{36}$$

Based on (30), (32), (33), and (35), one obtains a characteristic equation:

$$[H]_{\overline{n}\times\overline{n}} \{C\}_{\overline{n}\times 1} = 0, \tag{37}$$

where $\{C\}_{\overline{n}\times 1}$ is a $\overline{n} \times 1$ column vector composed of $\overline{n} = 2p$ integration constants for the τth mode shape of the pth rod segments, $C_{1,i}^{(\tau)}$ and $C_{2,i}^{(\tau)}$ ($i = 1, \ldots, i, \ldots, p$), that is,

$$\{C\}_{\overline{n}\times 1} = \begin{bmatrix} C_{1,1}^{(\tau)} & C_{2,1}^{(\tau)} & \cdots & C_{1,i}^{(\tau)} & C_{2,i}^{(\tau)} & \cdots & C_{1,p}^{(\tau)} & C_{2,p}^{(\tau)} \end{bmatrix}^T, \tag{38}$$

and $[H]_{\overline{n}\times\overline{n}}$ is a $\overline{n} \times \overline{n}$ (with $\overline{n} = 2p$) square matrix with its nonzero coefficients given by

$$H_{1,1} = \left[-\frac{3}{2}\beta_\tau z_{\tau,0}^{-1} + f_{\tau,0} \right] J_{3/2}(z_{\tau,0}) + \beta_\tau J'_{3/2}(z_{\tau,0}), \tag{39a}$$

$$H_{1,2} = \left[-\frac{3}{2}\beta_\tau z_{\tau,0}^{-1} + f_{\tau,0} \right] J_{-3/2}(z_{\tau,0}) + \beta_\tau J'_{-3/2}(z_{\tau,0}), \tag{39b}$$

$$H_{2i,2(i-1)+1} = J_{3/2}(z_{\tau,i}), \tag{40a}$$

$$H_{2i,2(i-1)+2} = J_{-3/2}(z_{\tau,i}), \tag{40b}$$

$$H_{2i,2(i-1)+3} = -J_{3/2}(z_{\tau,i}), \tag{40c}$$

$$H_{2i,2(i-1)+4} = -J_{-3/2}(z_{\tau,i}), \tag{40d}$$

$$H_{2i+1,2(i-1)+1} = \left[-\frac{3}{2}\beta_\tau z_{\tau,i}^{-1} - f_{\tau,i} \right] J_{3/2}(z_{\tau,i}) + \beta_\tau J'_{3/2}(z_{\tau,i}), \tag{41a}$$

$$H_{2i+1,2(i-1)+2} = \left[-\frac{3}{2}\beta_\tau z_{\tau,i}^{-1} - f_{\tau,i} \right] J_{-3/2}(z_{\tau,i}) + \beta_\tau J'_{-3/2}(z_{\tau,i}), \tag{41b}$$

$$H_{2i+1,2(i-1)+3} = \beta_\tau \left[\frac{3}{2} z_{\tau,i}^{-1} J_{3/2}(z_{\tau,i}) - J'_{3/2}(z_{\tau,i}) \right], \tag{41c}$$

$$H_{2i+1,2(i-1)+4} = \beta_\tau \left[\frac{3}{2} z_{\tau,i}^{-1} J_{-3/2}(z_{\tau,i}) - J'_{-3/2}(z_{\tau,i}) \right], \tag{41d}$$

$$H_{\overline{n},\overline{n}-1} = \left[-\frac{3}{2}\beta_\tau z_{\tau,p}^{-1} - f_{\tau,p} \right] J_{3/2}(z_{\tau,p}) + \beta_\tau J'_{3/2}(z_{\tau,p}), \tag{42a}$$

$$H_{\overline{n},\overline{n}} = \left[-\frac{3}{2}\beta_\tau z_{\tau,p}^{-1} - f_{\tau,p} \right] J_{-3/2}(z_{\tau,p}) + \beta_\tau J'_{-3/2}(z_{\tau,p}). \tag{42b}$$

For the case of a P-taper shaft consisting of one shaft segment (i.e., $p = 1$), only (39a), (39b), (42a), and (42b) are required for the determination of natural frequencies and associated mode shapes, and (40a)–(40d) and (41a)–(41d) are further required for the case of total number of shaft segments being greater than 1 (i.e., $p > 1$) with i being less than or equal to $p - 1$ (i.e., $i \le (p - 1)$).

Nontrivial solution of (37) requires that

$$|H| = 0. \tag{43}$$

Equation (43) is the frequency equation for the free-free P-taper shaft with each node i carrying one rigid disk $\widehat{J}_i$ and one torsional spring $\widehat{k}_{t,i}$ ($i = 0, 1, 2, \ldots, p$). From (43), one may find the natural frequencies of the vibrating system, ω_τ ($\tau = 1, 2, 3, \ldots$), and then, with respect to each natural frequency ω_τ, one may determine the values of $C_{1,i}^{(\tau)}$ and $C_{2,i}^{(\tau)}$ ($i = 1, 2, \ldots, p$) from (37). Finally, the substitution of the last integration constants into (26a) will determine the corresponding natural mode shape of the entire conic shaft $\Theta_\tau(x)$. Since the values of rotary inertia $\widehat{J}_i$ and rotational stiffness $\widehat{k}_{t,i}$ are arbitrary including zero, the foregoing formulation is available for arbitrary cases of the free-free loaded conic shaft including the bare one.

For the special case of a free-free conic shaft consisting of only one shaft segment (i.e., $p = 1$), (37) reduces to

$$[H]_{2\times 2} \{C\}_{2\times 1} = 0, \tag{44}$$

where

$$\{C\}_{2\times 1} = \left[C_{1,1}^{(\tau)} \; C_{2,1}^{(\tau)}\right]^T, \tag{45a}$$

$$[H]_{2\times 2} = \begin{bmatrix} H_{1,1} & H_{1,2} \\ H_{2,1} & H_{2,2} \end{bmatrix}. \tag{45b}$$

In (45b), the coefficients $H_{1,1}$ and $H_{1,2}$ are the same as those given by (39a) and (39b), while those $H_{2,1}$ and $H_{2,2}$ may be obtained from (42a) and (42b) by letting $p = 1$ and $\overline{n} = 2p = 2$. The results are

$$H_{2,1} = \left[-\frac{3}{2}\beta_\tau z_{\tau,1}^{-1} - f_{\tau,1}\right] J_{3/2}\left(z_{\tau,1}\right) + \beta_\tau J_{3/2}'\left(z_{\tau,1}\right), \tag{46a}$$

$$H_{2,2} = \left[-\frac{3}{2}\beta_\tau z_{\tau,1}^{-1} - f_{\tau,1}\right] J_{-3/2}\left(z_{\tau,1}\right) + \beta_\tau J_{-3/2}'\left(z_{\tau,1}\right), \tag{46b}$$

where

$$z_{\tau,1} = \beta_\tau x_p = \beta_\tau L_\ell. \tag{47}$$

5.2. Clamped-Clamped P-Taper Conic Shaft. If both left and right ends of the P-taper conic shaft shown in Figure 2 are clamped, then the effects of all concentrated elements at the last two ends are nil. In such a case, the foregoing nonclassical boundary conditions of the conic shaft are the same as the C-C classical ones given by (23a) and (23b). Substitution of (26a) into (23a) and (23b), respectively, yields

$$C_{1,1}^{(\tau)} J_{3/2}\left(z_{\tau,0}\right) + C_{2,1}^{(\tau)} J_{-3/2}\left(z_{\tau,0}\right) = 0, \tag{48a}$$

$$C_{1,p}^{(\tau)} J_{3/2}\left(z_{\tau,p}\right) + C_{2,p}^{(\tau)} J_{-3/2}\left(z_{\tau,p}\right) = 0. \tag{48b}$$

Therefore, the coefficients relating to the boundary conditions, given by (39a), (39b), (42a), and (42b), must be, respectively, replaced by

$$H_{1,1} = J_{3/2}\left(z_{\tau,0}\right), \tag{49a}$$

$$H_{1,2} = J_{-3/2}\left(z_{\tau,0}\right), \tag{49b}$$

$$H_{\overline{n},\overline{n}-1} = J_{3/2}\left(z_{\tau,p}\right), \tag{50a}$$

$$H_{\overline{n},\overline{n}} = J_{-3/2}\left(z_{\tau,p}\right). \tag{50b}$$

5.3. Clamped-Free (or Free-Clamped) P-Taper Conic Shaft. The formulation presented in Section 5.1 is also available for the free vibration analysis of the clamped-free (C-F) and free-clamped (F-C) P-taper conic shaft: the BCs given by (49a), (49b), (42a), and (42b) are required for a C-F shaft, and the BCs given by (39a), (39b), (50a), and (50b) are required for a F-C shaft. It is noted that, for the classical boundary conditions, $\hat{J}_0 = \hat{k}_{t,0} = 0$ and $\hat{J}_p = \hat{k}_{t,p} = 0$.

6. Formulation for a PN-Taper Conic Shaft

Figure 3 shows the coordinate system of a conic shaft composed of a shaft segment $\overline{AB}$ with positive taper and a shaft segment $\overline{BC}$ with negative taper, which is called *PN-taper* conic shaft in this paper. The key parameters for the positive-taper part $\overline{AB}$, d_s, d_ℓ, L_s and L_ℓ, are the same as those shown in Figures 1 or 2 for the P-taper conic shaft, and the corresponding ones of the negative-taper part $\overline{BC}$ are represented by $\overline{d}_s$, $\overline{d}_\ell$, $\overline{L}_s$, and $\overline{L}_\ell$, respectively. Since the origin $\overline{o}$ for the coordinate system of the negative-taper part $\overline{BC}$ is located at $x = L_\ell + \overline{L}_\ell$, the relationship between the axial coordinates $\overline{x}$ and x is given by

$$\overline{x} = \left(L_\ell + \overline{L}_\ell\right) - x \quad \left(\text{for } L_\ell \le x \le \left(L_\ell + \overline{L}_\ell - \overline{L}_s\right)\right). \tag{51}$$

If the intermediate node i is located at the junction of positive-taper part $\overline{AB}$ and negative-taper part $\overline{BC}$ of the PN-taper conic shaft $\overline{ABC}$, that is, $x = x_i = L_\ell$, then (16a), (16b), (33), (41c), and (41d) must be, respectively, replaced by

$$\Theta_{\tau,i}\left(z_{\tau,i}\right) = \Theta_{\tau,i+1}\left(\overline{z}_{\tau,i}\right), \tag{52a}$$

$$\begin{aligned} GI_{p,i}\Theta_{\tau,i}'\left(z_{\tau,i}\right) = & -G\overline{I}_{p,i+1}\Theta_{\tau,i+1}'\left(\overline{z}_{\tau,i}\right) \\ & + \left(\omega_\tau^2 \hat{J}_i - \hat{k}_{t,i}\right)\Theta_{\tau,i}\left(z_{\tau,i}\right), \end{aligned} \tag{52b}$$

$$\begin{aligned} & C_{1,i}^{(\tau)}\left\{\left[-\frac{3}{2}\beta_\tau z_{\tau,i}^{-1} - f_{\tau,i}\right] J_{3/2}\left(z_{\tau,i}\right) + \beta_\tau J_{3/2}'\left(z_{\tau,i}\right)\right\} \\ & + C_{2,i}^{(\tau)}\left\{\left[-\frac{3}{2}\beta_\tau z_{\tau,i}^{-1} - f_{\tau,i}\right] J_{-3/2}\left(z_{\tau,i}\right) + \beta_\tau J_{-3/2}'\left(z_{\tau,i}\right)\right\} \\ & - C_{1,i+1}^{(\tau)} R_I \beta_\tau \left[\frac{3}{2}\overline{z}_{\tau,i}^{-1} J_{3/2}\left(\overline{z}_{\tau,i}\right) - J_{3/2}'\left(\overline{z}_{\tau,i}\right)\right] \\ & - C_{2,i+1}^{(\tau)} R_I \beta_\tau \left[\frac{3}{2}\overline{z}_{\tau,i}^{-1} J_{-3/2}\left(\overline{z}_{\tau,i}\right) - J_{-3/2}'\left(\overline{z}_{\tau,i}\right)\right] = 0, \end{aligned} \tag{53}$$

$$H_{2i+1,2(i-1)+3} = -R_I \beta_\tau \left[\frac{3}{2}\overline{z}_{\tau,i}^{-1} J_{3/2}\left(\overline{z}_{\tau,i}\right) - J_{3/2}'\left(\overline{z}_{\tau,i}\right)\right], \tag{54a}$$

$$H_{2i+1,2(i-1)+4} = -R_I \beta_\tau \left[\frac{3}{2}\overline{z}_{\tau,i}^{-1} J_{-3/2}\left(\overline{z}_{\tau,i}\right) - J_{-3/2}'\left(\overline{z}_{\tau,i}\right)\right], \tag{54b}$$

where

$$\bar{x}_i = \left(L_1 + \bar{L}_1\right) - x_i, \tag{55a}$$

$$z_{\tau,i} = \beta_\tau x_i, \tag{55b}$$

$$\bar{z}_{\tau,i} = \beta_\tau \bar{x}_i, \tag{55c}$$

$$I_{p,i} = \left(\frac{x_i}{L_\ell}\right)^4 I_{p,\ell}, \tag{55d}$$

$$\bar{I}_{p,i+1} = \left(\frac{\bar{x}_i}{\bar{L}_\ell}\right)^4 \bar{I}_{p,\ell}, \tag{55e}$$

$$R_I = \frac{\bar{I}_{p,i+1}}{I_{p,i}}. \tag{55f}$$

Furthermore, if the intermediate node i is located at the negative-taper part $\overline{BC}$ of the PN-taper conic shaft $\overline{ABC}$, that is, $x = x_i > L_\ell$, then (34) and (36) must be, respectively, replaced by

$$f_{\tau,i} = \frac{-\left(\omega_\tau^2 \hat{J}_i - \hat{k}_{t,i}\right)}{\left(GI_{p,i}\right)}, \tag{56}$$

$$f_{\tau,p} = \frac{-\left(\omega_\tau^2 \hat{J}_p - \hat{k}_{t,p}\right)}{\left(GI_{p,p}\right)}. \tag{57}$$

The negative signs (−) in the right hand sides of (52b), (56), and (57) are due to the fact that the sign for the first derivative of the negative-taper part $\overline{BC}$ of the PN-taper shaft is opposite to that of the positive-taper part $\overline{AB}$ (cf. Figure 3), that is, $d/d\bar{x} = -d/dx$ according to (51).

It is noted that the formulation for the P-taper conic shaft presented in the last section is available for the positive-taper part $\overline{AB}$ of the current PN-taper conic shaft $\overline{ABC}$, and so is for the negative-taper part $\overline{BC}$, if one obtains the axial coordinate $\bar{x}$ from (51) and sets

$$x = \bar{x}, \tag{58a}$$

$$d_s = \bar{d}_s, \tag{58b}$$

$$d_\ell = \bar{d}_\ell, \tag{58c}$$

$$L_s = \bar{L}_s, \tag{58d}$$

$$L_\ell = \bar{L}_\ell \tag{58e}$$

for the intermediate node i located in the negative-taper part $\overline{BC}$, that is, for the case of $L_\ell < x = x_i \le (L_\ell + \bar{L}_\ell - \bar{L}_s)$.

7. Free Torsional Vibration Analysis of a Conic Shaft by FEM

In order to use the conventional FEM to tackle the examined problem, the conic shaft such as that shown in Figure 3 must be replaced by a stepped one composed of n_e uniform circular shaft elements shown in Figure 4(a). The average diameter of the jth uniform shaft segment, $\tilde{d}_j$, is determined in the following.

From Figure 4(b), one sees that the diameters for the cross-sections of the original conic shaft located at the two ends of the jth uniform rod element, d_k and d_{k+1}, are given by

$$d_j = \left(\frac{x_j}{L_\ell}\right) d_\ell, \tag{59a}$$

$$d_{j+1} = \left(\frac{x_{j+1}}{L_\ell}\right) d_\ell, \tag{59b}$$

Based on the requirement that the mass of the jth uniform shaft element (with average diameter $\tilde{d}_j$) is equal to that of its original jth conic shaft element, one obtains

$$\rho\left(\frac{\pi \tilde{d}_j^2}{4}\right)\ell_j = \frac{1}{3}\frac{\rho\pi\left(d_{j+1}^2 x_{j+1} - d_j^2 x_j\right)}{4}. \tag{60}$$

From the last expression, one obtains average diameter of the jth uniform shaft element

$$\tilde{d}_j = \sqrt{\frac{\left(d_{j+1}^2 x_{j+1} - d_j^2 x_j\right)}{\left(3\ell_j\right)}}, \tag{61}$$

where

$$\ell_j = \Delta x_j = \frac{L_{\text{shaft}}}{n_e}. \tag{62}$$

Therefore, the average polar moment of inertia for the cross-sectional area of the jth uniform shaft element is given by

$$\tilde{I}_{p,j} = \frac{\pi \tilde{d}_j^4}{32}, \tag{63}$$

and the corresponding polar mass moment of inertia J_j of the jth uniform shaft element is determined by

$$J_j = \rho \ell_j \tilde{I}_{p,j}. \tag{64}$$

Equations (59a)–(61) are for the case of the jth shaft element being located in the positive-taper part $\overline{AB}$ of the PN-taper

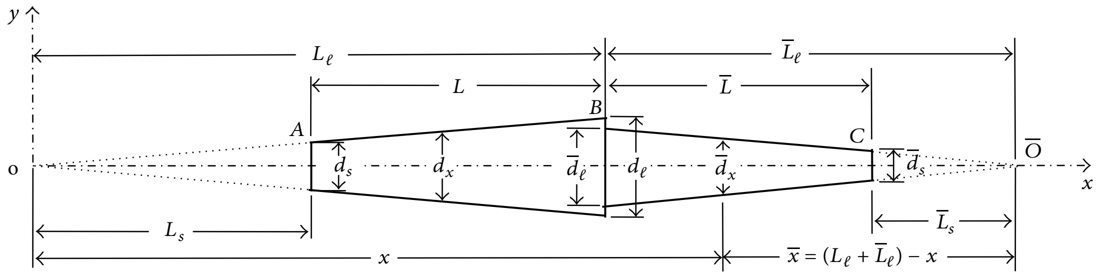

FIGURE 3: The coordinate system for PN-taper conic shaft ($\overline{ABC}$) composed of both a positive-taper part $\overline{AB}$ and a negative-taper part $\overline{BC}$.

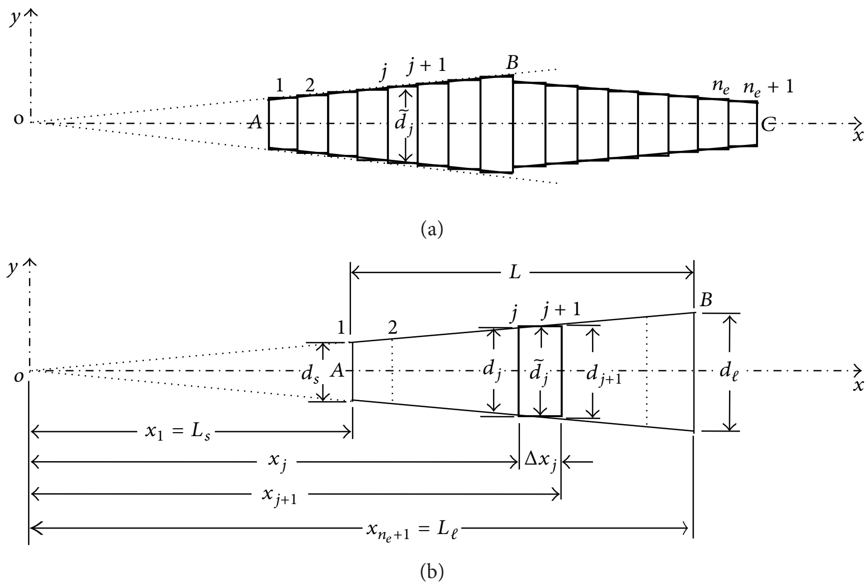

FIGURE 4: (a) The PN-taper conic shaft ($\overline{ABC}$) is replaced by n_e uniform circular shaft elements. (b) The average diameter $\tilde{d}_j$ ($j = 1, 2, \ldots, n_e$) for the jth uniform circular shaft element in the positive-taper part $\overline{AB}$ is determined by $\tilde{d}_j = \sqrt{(d_{j+1}^2 x_{j+1} - d_j^2 x_j)/(3\Delta x_j)}$.

conic shaft $\overline{ABC}$. If the jth shaft element is located in the negative-taper part $\overline{BC}$, then (59a)–(61) must be, respectively, replaced by

$$\bar{d}_j = \left(\frac{\bar{x}_j}{\bar{L}_\ell}\right)\bar{d}_\ell, \qquad (59\text{a})'$$

$$\bar{d}_{j+1} = \left(\frac{\bar{x}_{j+1}}{\bar{L}_\ell}\right)\bar{d}_\ell, \qquad (59\text{b})'$$

$$\rho\left(\frac{\pi\tilde{d}_j^2}{4}\right)\ell_j = \frac{1}{3}\frac{\rho\pi\left(\bar{d}_j^2\bar{x}_j - \bar{d}_{j+1}^2\bar{x}_{j+1}\right)}{4}, \qquad (60)'$$

$$\tilde{d}_j = \sqrt{\frac{\left(\bar{d}_j^2\bar{x}_j - \bar{d}_{j+1}^2\bar{x}_{j+1}\right)}{\left(3\ell_j\right)}}. \qquad (61)'$$

In the last expressions, the values of $\bar{x}_j$ and $\bar{x}_{j+1}$ are determined by (51).

Based on the foregoing information for the jth uniform rod element ($j = 1, 2, 3, \ldots, n_e$) and shear modulus G of the shaft material, one may obtain the mass matrix and stiffness matrix of each uniform shaft element from [12]:

$$[m]_j = J_j \begin{bmatrix} \frac{1}{3} & \frac{1}{6} \\ \frac{1}{6} & \frac{1}{3} \end{bmatrix}, \qquad (65\text{a})$$

$$[k]_j = \left(\frac{G\tilde{I}_{p,j}}{\ell_j}\right)\begin{bmatrix} 1 & -1 \\ -1 & 1 \end{bmatrix}. \qquad (65\text{b})$$

Assembly of the elemental mass and stiffness matrices for each of the uniform shaft elements yields the overall mass matrix $[m]$ and overall stiffness matrix $[k]$ of the entire conic shaft. If there exist a rigid disk with rotary inertia $\hat{J}_j$ and a torsional spring with stiffness $\hat{k}_{t,j}$ at $x = x_j$, then $\hat{J}_j$ and $\hat{k}_{t,j}$ must be added to the jth diagonal coefficient of the overall mass matrix $[m]$ and that of the overall stiffness matrix $[k]$, respectively. Finally, imposing the specified boundary conditions of the entire conic shaft and solving the resulting characteristic equation, one will determine the natural frequencies and the corresponding mode shapes of the entire conic shaft.

8. Numerical Results and Discussions

Except Tables 2 and 3, all numerical results for the P-taper conic shaft (cf. Figures 1 or 2) in this paper are based on the following data (cf. case 2 of Table 1): mass density $\rho = 7850\,\mathrm{kg/m^3}$, Young's modulus $E = 2.068 \times 10^{11}\,\mathrm{N/m^2}$, shear modulus $G = E/[2(1+\nu)] = 0.7953846 \times 10^{11}\,\mathrm{N/m^2}$, Poison's ratio $\nu = 0.3$, smaller-end diameter $d_s = 0.03\,\mathrm{m}$, larger-end diameter $d_\ell = 0.05\,\mathrm{m}$, and distance from origin o to the smaller end $L_s = 3.0\,\mathrm{m}$ and that to the larger end $L_\ell = 5.0\,\mathrm{m}$. The parameters for the negative-taper part $\overline{BC}$ of the PN-taper shaft $\overline{ABC}$ (cf. Figure 3) are the same as the corresponding ones of positive-taper part $\overline{AB}$, that is, $\overline{d}_s = d_s$, $\overline{d}_\ell = d_\ell$, $\overline{L}_s = L_s$, and $\overline{L}_\ell = L_\ell$. For convenience, two reference parameters are introduced:

$$J^* = \rho \widetilde{I}_P L_{\mathrm{shaft}}, \tag{66a}$$

$$k_t^* = \frac{G\widetilde{I}_P}{L_{\mathrm{shaft}}}, \tag{66b}$$

where J^* denotes the reference polar mass moment of inertia for rigid disks and k_t^* denotes the reference stiffness for torsional springs, L_{shaft} denotes the length of the entire shaft and is given by $L_{\mathrm{shaft}} = L_\ell - L_s$ for the P-taper shaft and $L_{\mathrm{shaft}} = (L_\ell + \overline{L}_\ell) - (L_s + \overline{L}_s)$ for PN-taper shaft; besides, $\widetilde{I}_p$ denotes the average polar moment of inertia for the entire taper shaft, that is,

$$\widetilde{I}_p = \frac{\left(I_{p,s} + I_{p,\ell}\right)}{2} \quad (\text{for the P-taper shaft}), \tag{67a}$$

$$\widetilde{I}_p = \frac{\left(I_{p,s} + I_{p,\ell} + \overline{I}_{p,s} + \overline{I}_{p,\ell}\right)}{4} \quad (\text{for the PN-taper shaft}), \tag{67b}$$

where $I_{p,s}$ and $I_{p,\ell}$ denote the polar moment of inertia of the smaller-end area and that of the larger-end area of the P-taper shaft (or the positive-taper part $\overline{AB}$ of the PN-taper shaft $\overline{ABC}$), respectively, while $\overline{I}_{p,s}$ and $\overline{I}_{p,\ell}$ denote the corresponding ones of the negative-taper part $\overline{BC}$ of the PN-taper shaft. Based on the foregoing given data, one obtains the reference polar mass moment of inertia $J^* = 5.4409436902 \times 10^{-3}\,\mathrm{kg\text{-}m^2}$ and reference stiffness $k_t^* = 1.378230198 \times 10^4\,\mathrm{N{\cdot}m/rad}$ for the P-taper shaft. Because the dimensions of the positive-taper part $\overline{AB}$ of the PN-taper shaft $\overline{ABC}$ are identical to those of the P-taper shaft and the dimensions of the negative-taper part $\overline{BC}$ of the PN-taper shaft $\overline{ABC}$ are the same as the positive-taper part $\overline{AB}$, it is evident that the reference polar mass moment of inertia $J^* = 2 \times 5.4409436902 \times 10^{-3}\,\mathrm{kg{\cdot}m^2}$ and reference stiffness $k_t^* = (1.378230198 \times 10^4)/2\,\mathrm{N{\cdot}m/rad}$ for the PN-taper shaft.

8.1. Influence of Taper Ratios on the P-Taper Shaft. In this paper, the taper ratio $\overline{\alpha}$ of the conic shaft is defined by $\overline{\alpha} = d_\ell/L_\ell = d_s/L_s$, and the five cases of taper ratio and the associated parameters of the P-taper shaft are shown in Table 1. Furthermore, the sketch for the P-taper shaft with taper ratios $\overline{\alpha} = 0.02, 0.01, 0.005, 0.0025$, and 0.001 is shown in Figure 5 with diameter of the larger end ($d_\ell = 0.05\,\mathrm{m}$) and length of the shaft ($L_{\mathrm{shaft}} = L = 2.0\,\mathrm{m}$) being kept unchanged. The influence of taper ratio $\overline{\alpha}$ on the lowest five natural frequencies of the P-taper shaft, ω_τ ($\tau = 1$ to 5), is shown in Tables 2(a), 2(b), 2(c), and 2(d) for the F-F, C-C, C-F, and F-C BCs, respectively. In which, *Exact* refers to the exact method presented in this paper, *FEM* refers to the conventional finite element method and the natural frequencies of the uniform shaft listed in the final row of each table (and denoted by the bold-faced digits) are obtained from the formulas given in the appendix at the end of this paper. From Tables 2(a)–2(d), one finds that:

(i) For various BCs, the lowest five natural frequencies (ω_τ, $\tau = 1$ to 5) of the P-taper shaft obtained from either exact method (using single shaft segment, i.e., $p = 1$) or FEM (using 50 shaft elements, i.e., $n_e = 50$) converge to the corresponding ones of the uniform circular shaft obtained from the exact formulas given in the appendix, when the taper ratio $\overline{\alpha}$ decreases and approaches zero.

(ii) For various BCs, the lowest five natural frequencies of the P-taper shaft obtained from the exact method (using $p = 1$) are very close to those obtained from FEM (using $n_e = 50$).

(iii) For the F-F, C-C, or F-C BCs, the lowest five natural frequencies (ω_τ, $\tau = 1$ to 5) of the P-taper shaft decrease with the decrease of taper ratio $\overline{\alpha}$ as one may see from Tables 2(a), 2(b), and 2(d). This is a reasonable result because the influence of taper ratio $\overline{\alpha}$ on the supporting stiffness is very small for the above-mentioned BCs (with right-end clamped and diameter being kept unchanged) and the polar mass moment of inertia of the entire shaft increases with the decrease of taper ratio $\overline{\alpha}$.

(iv) For the C-F BCs (cf. Table 2(c)), the lowest two to five natural frequencies (ω_2 to ω_5) of the P-taper shaft also decrease with the decrease of taper ratio $\overline{\alpha}$. However, the first natural frequency ω_1 increases significantly with the decrease of the taper ratio $\overline{\alpha}$. This is also a reasonable result because, near the (left) clamped end, the increasing effect of supporting stiffness is much greater than that of polar mass moment of inertia due to the decrease of taper ratio $\overline{\alpha}$.

Based on the foregoing reasonable results, it is believed that the theory and computer programs developed for the presented exact method should be reliable. It is worthy of mention that because the exact solution of the current research is determined based on the bar theory [7], the beam element theory [12] is used in FEM. The fundamental theory of solid element is different from the bar theory. Therefore, the solid element is not adopted in FEM.

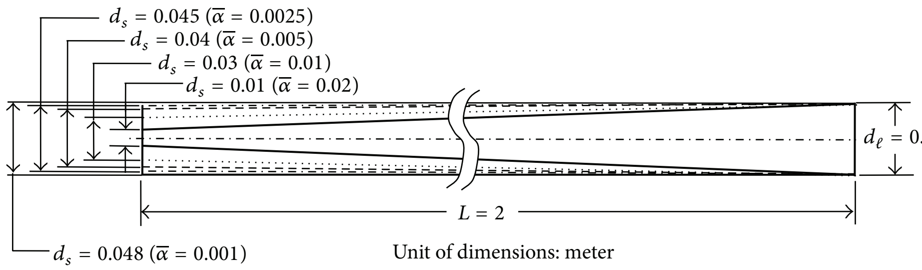

FIGURE 5: The profiles for longitudinal cross-sections of the conic shaft with five different taper ratios (cf. Table 1).

8.2. Influence of Taper Ratios on the PN-Taper Shaft. For the PN-taper shaft $\overline{ABC}$ as shown in Figures 3 or 4(a), if the dimensions of its positive-taper part $\overline{AB}$ are the same as those of the P-taper shaft (cf. Figure 5) studied in the last (Section 8.1), and the dimensions of the negative-taper part $\overline{BC}$ are identical to the corresponding ones of the positive-taper part $\overline{AB}$, then the influence of taper ratio $\overline{\alpha}$ on the lowest five natural frequencies (ω_τ, $\tau = 1$ to 5) of the PN-taper shaft is shown in Tables 3(a), 3(b), and 3(c) for the F-F, C-C, and C-F (or F-C) BCs, respectively. From Table 3, one sees that:

(i) for various BCs, the lowest five natural frequencies (ω_τ, $\tau = 1$ to 5) of the PN-taper shaft obtained from either exact method (using two shaft segments, i.e., $p = 2$) or FEM (using 100 shaft elements, i.e., $n_e = 100$) converge to the corresponding ones of the uniform circular shaft (cf. bold-faced digits in the final row of each table) obtained from the exact formulas given in the appendix, when the taper ratio $\overline{\alpha}$ decreases and approaches zero.

(ii) For various BCs, the lowest five natural frequencies of the PN-taper shaft obtained from the exact method (using $p = 2$) are very close to those obtained from FEM (using $n_e = 100$).

(iii) Because of symmetry in geometrical structures, the lowest five natural frequencies of the C-F PN-taper shaft are identical to those of F-C PN-taper shaft.

(iv) Comparing Table 3(b) with Table 2(c), one sees that the 1st, 3rd, and 5th natural frequencies of the PN-taper shaft (with C-C BCs) are exactly equal to the 1st, 2nd, and 3rd natural frequencies of the P-taper shaft (with C-F BCs), respectively. This is because the dimensions and left-end boundary conditions of the positive-taper part $\overline{AB}$ of the PN-taper shaft $\overline{ABC}$ are the same as those of the P-taper shaft, and the 1st, 3rd, and 5th mode shapes of the former are the same as the 1st, 2nd, and 3rd mode shapes of the latter, respectively.

In view of the foregoing reasonable results, one believes that the theory and computer programs developed for the PN-taper shaft should be reliable.

8.3. A Free-Free P-Taper Shaft Carrying Multiple Concentrated Elements. To show the ability of the presented exact method for obtaining the exact solution of free torsional vibration of the conic shaft carrying arbitrary concentrated elements, the lowest five natural frequencies and some associated mode shapes of a free-free P-taper shaft carrying 3 identical rigid disks and 3 identical torsional springs (cf. Figure 6) are determined in this subsection. The taper ratio of the P-taper shaft is $\overline{\alpha} = d_\ell/L_\ell = 0.01$. From case 2 of Table 1, one sees that the pertinent parameters for the current P-taper shaft are: diameter at smaller end $d_s = 0.03$ m, diameter at larger end $d_\ell = 0.05$ m, coordinate at smaller end $x_0 = L_s = 3.0$ m, and coordinate at larger end $x_p = L_\ell = 5.0$ m. It is noted that the origin of the last coordinates is at the tip of the conic shaft (cf. Figure 6). In Figure 6(a), the P-taper shaft carries 3 identical rigid disks, where the polar mass moment of inertia of each disk is given by $\widehat{J}_i = J^*/3$ ($i = 0, 1, 2$) with $J^* = 5.4409436902\times10^{-3}$ kg-m^2 denoting the reference polar mass moment of inertia mentioned at the beginning of the current section. In Figure 6(b), the P-taper shaft carries 3 identical torsional springs, where the stiffness of each torsional spring is given by $\widehat{k}_{t,i} = k_t^*/3$ ($i = 0, 1, 2$) with $k_t^* = 1.378230198 \times 10^4$ Nm/rad denoting the reference stiffness mentioned at the beginning of the current section. In Figure 6(c), the 3 identical rigid disks shown in Figure 6(a) and the 3 identical torsional springs shown in Figure 6(b) are attached to the same P-taper shaft. The locations of the concentrated elements (rigid disks or torsional springs or both rigid disks and torsional springs) are $x_0 = 3.0$ m, $x_1 = 4.0$ m, and $x_2 = 5.0$ m, as one may see from Figure 6. For convenience, in Table 4, the loaded P-taper shaft shown in Figures 6(a), 6(b), and 6(c) are called cases 1, 2, and 3, respectively. Besides, the total number of rigid disks is denoted by $N_{\widehat{J}}$ and that of torsional springs by $N_{\widehat{k}_t}$ in the same table.

Comparing with the lowest four natural frequencies of the bare free-free P-taper shaft (without carrying any concentrated elements) given by case 2 of Table 2(a) and listed in the final row of Table 4 (denoted by the bold-faced digits), one sees that the 3 identical rigid disks, each with $\widehat{J}_i = J^*/3$ ($i = 0, 1, 2$) as shown in Figure 6(a), reduce the lowest four natural frequencies of the P-taper shaft (cf. case 1 in Table 4). On the contrary, the 3 identical torsional springs, each with $\widehat{k}_{t,i} = k_t^*/3$ ($i = 0, 1, 2$) as shown in Figure 6(b), raise the lowest four natural frequencies of the P-taper shaft (cf. case 2 in Table 4). When the last concentrated elements are simultaneously attached to the P-taper shaft as shown in Figure 6(c), it is under expectation that the numerical values

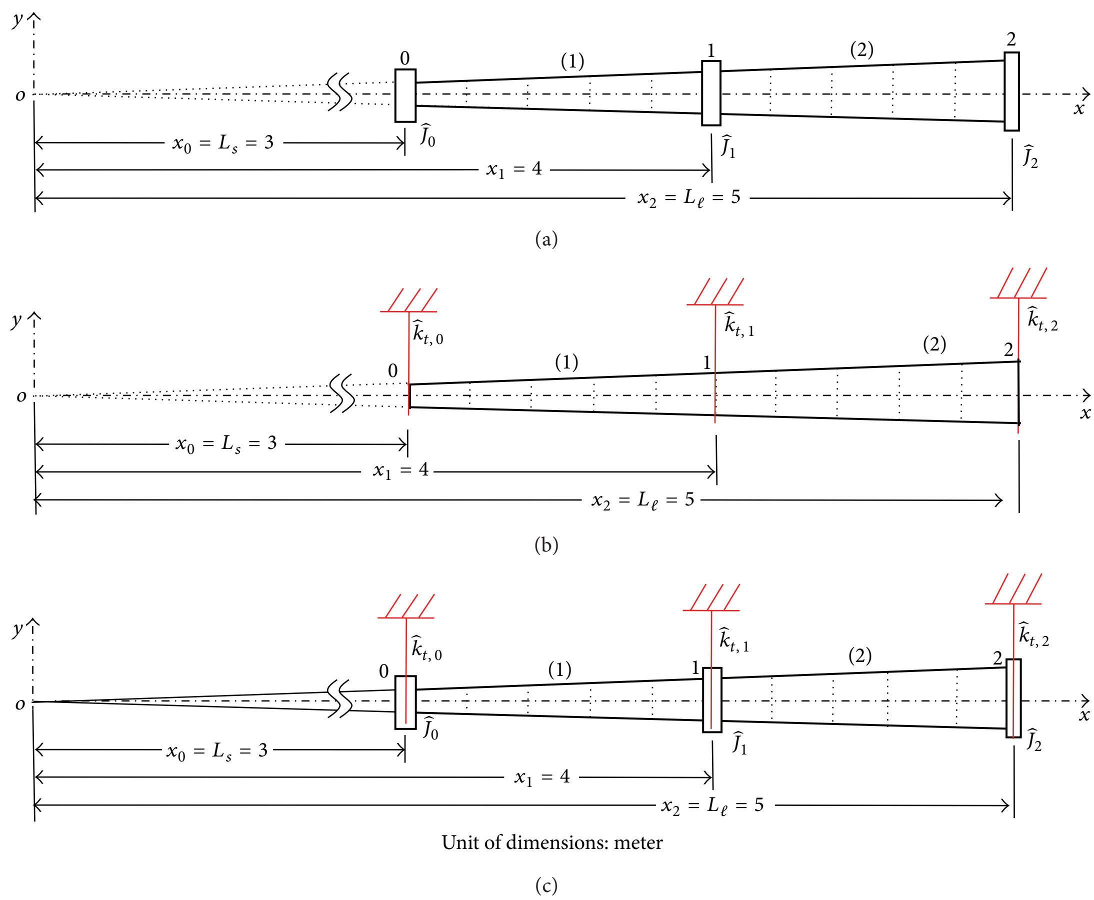

Figure 6: The P-taper shaft (cf. case 2 of Table 1) carrying: (a) 3 rigid disks each with $\hat{J}_i = J^*/3$ $(i = 0, 1, 2)$; (b) 3 torsional springs each with $\hat{k}_{t,i} = k_t^*/3$ $(i = 0, 1, 2)$; and (c) 3 rigid disks and 3 torsional springs each with $\hat{J}_i = J^*/3$ and $\hat{k}_{t,i} = k_t^*/3$ $(i = 0, 1, 2)$. The locations of concentrated elements are $x_0 = 3.0$ m, $x_1 = 4.0$ m, and $x_2 = 5.0$ m. Besides, $J^* = 5.4409436902 \times 10^{-3}$ kg-m^2 and $k_t^* = 1.378230198 \times 10^4$ Nm/rad.

of the lowest four natural frequencies of the shaft have the next relationship: $\omega_{i,(a)} < \omega_{i,(c)} < \omega_{i,(b)}$, where $\omega_{i,(a)}$, $\omega_{i,(b)}$, and $\omega_{i,(c)}$ represent the ith natural frequencies of the P-taper shafts shown in Figures 6(a), 6(b), and 6(c), respectively.

It is noted that, for a free-free shaft supported by torsional springs such as that shown in Figures 6(b) or 6(c), there exists a quasi rigid-body natural frequency ω_0 as one may see from Table 4. The quasi straight lines (—⧫— and - -◊- -) appearing in the upper side of Figure 7(b) are the mode shapes corresponding to the above-mentioned frequencies ω_0 for the shaft shown in Figure 6(c), obtained from the presented exact method and the conventional FEM, respectively. For a true rigid shaft, its natural frequency is given by $\overline{\omega}_0 = \sqrt{k_t/J}$; thus, the true rigid body natural frequency for the P-taper shaft shown in Figure 6(b) is given by $\overline{\omega}_{0,(b)} = \sqrt{k_t^*/J^*} = \sqrt{1.378230198 \times 10^4/5.44094369 \times 10^{-3}} =$ 1591.5627 rad/sec, and that shown in Figure 6(c) by $\overline{\omega}_{0,(c)} = \sqrt{k_t^*/(2J^*)} = \sqrt{1.378230198 \times 10^4/(2 \times 5.44094369 \times 10^{-3})}$ = 1125.4048 rad/sec, where $2J^*$ is the summation of polar mass moment of inertia of the entire shaft itself (J^*) and that of the 3 rigid disks (J^*). Comparing with cases 2 and 3 of Table 4, one sees that quasi rigid-body natural frequencies, $\omega_{0,(b)} = 1684.6341$ rad/sec and $\omega_{0,(c)} = 1168.6767$ rad/sec, are slightly greater than the foregoing corresponding true ones, $\overline{\omega}_{0,(b)} = 1591.5627$ rad/sec and $\overline{\omega}_{0,(c)} = 1125.4048$ rad/sec, respectively.

The lowest five mode shapes (including the quasi rigid-body mode) of the "loaded" free-free P-taper shaft shown in Figure 6(c) are plotted in Figure 7(b). Comparing with the corresponding ones of the "bare" free-free P-taper shaft shown in Figure 7(a), one sees that the lowest four (elastic) mode shapes of the "loaded" shaft are much different from those of the "bare" shaft. From Table 4, one sees that all the natural frequencies obtained from FEM using 50 shaft elements (i.e., $n_e = 50$) are very close to the corresponding ones obtained from the presented exact method using 2 shaft segments (i.e., $p = 2$).

In Figure 7, the mode shapes obtained from the presented exact method are represented by the solid lines (—) and those obtained from FEM by the dashed lines (- - -). Furthermore, the 1st, 2nd, 3rd, and 4th mode shapes obtained from the exact method are denoted by the symbols •, +, ▲, and ■, respectively, while those from FEM by

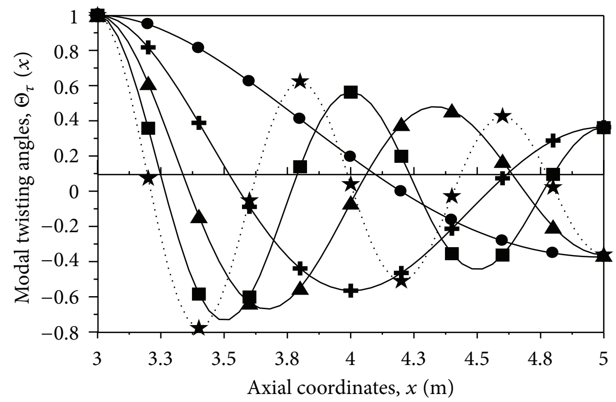

(a)

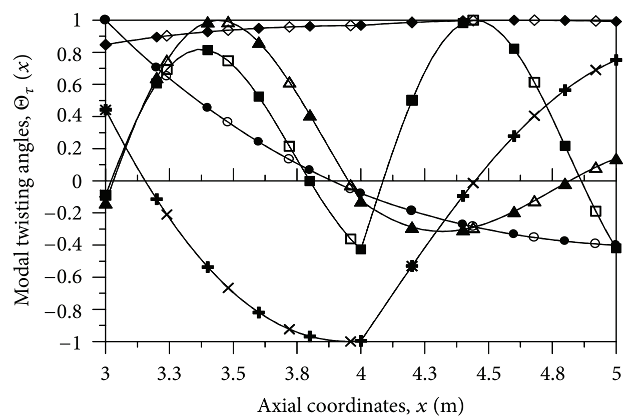

(b)

FIGURE 7: The lowest five mode shapes of the free-free P-taper shaft with taper ratio $\overline{\alpha} = 0.01$ (cf. case 2 of Table 1): (a) for the bare shaft (without any attachments as shown in Figure 1); (b) for the loaded shaft (carrying 3 rigid disks and 3 torsional springs as shown in Figure 6(c)).

the symbols $\circ$, $\times$, $\triangle$ and $\square$, respectively. Because all the natural frequencies obtained from FEM are very close to the corresponding ones obtained from the presented exact method as one may see from Table 4, so are the associated mode shapes obtained from the above two methods as shown in Figure 7(b).

8.4. A Free-Free PN-Taper Shaft Carrying Multiple Concentrated Elements. This subsection studies the free vibration characteristics of a free-free PN-taper shaft carrying 5 identical rigid disks and 5 identical torsional springs as shown in Figure 8 by using the presented exact method (with 4 shaft segments, i.e., $p = 4$) and the conventional FEM (with 100

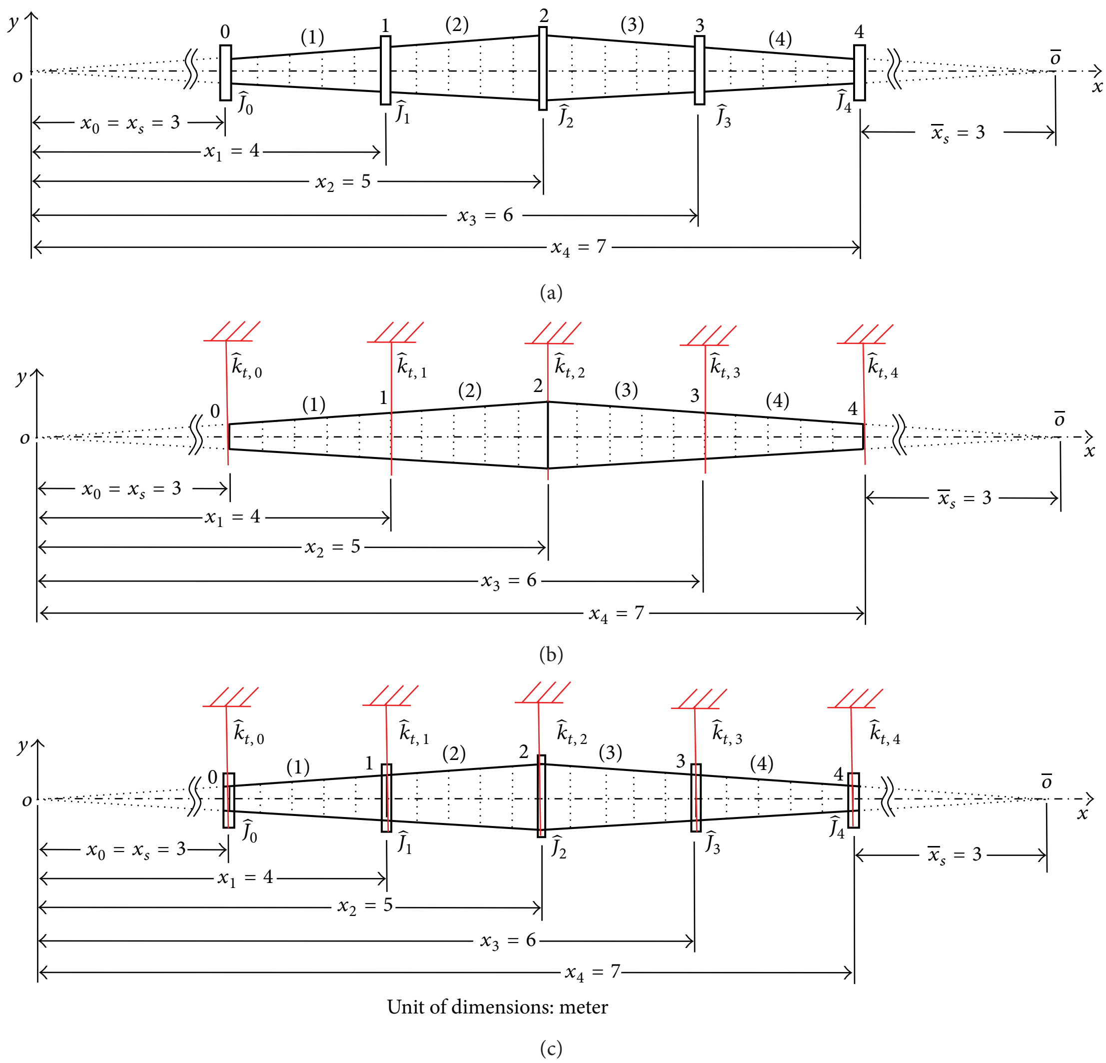

Figure 8: The free-free PN-taper conic shaft carrying: (a) 5 rigid disks each with $\hat{J}_i = J^*/5$ $(i = 0, 1, 2, 3, 4)$; (b) 5 torsional springs each with $\hat{k}_{t,i} = k_t^*/5$ $(i = 0, 1, 2, 3, 4)$; and (c) 5 rigid disks and 5 torsional springs each with $\hat{J}_i = J^*/5$ and $\hat{k}_{t,i} = k_t^*/5$ $(i = 0, 1, 2, 3, 4)$. The locations of the concentrated elements are: $x_i = 3.0$, 4.0, 5.0, 6.0, and 7.0 m, respectively. Besides, $J^* = 1.0881887380 \times 10^{-2}$ kg-m^2 and $k_t^* = 6.891150988 \times 10^3$ N-m/rad.

shaft elements, i.e., $n_e = 100$). The parameters for the positive-taper part $\overline{AB}$ of the current PN-taper shaft $\overline{ABC}$ are the same as those of the P-taper shaft studied in the last subsection, and the parameters for the negative-taper part $\overline{BC}$ are identical to the positive-taper part $\overline{AB}$, that is, $\overline{d}_s = d_s = 0.03$ m, $\overline{d}_\ell = d_\ell = 0.05$ m, $\overline{L}_s = L_s = 3.0$ m, and $\overline{L}_\ell = L_\ell = 5.0$ m. The polar mass moment of inertia for each of the 5 identical rigid disks is given by $\hat{J}_i = J^*/5$ $(i = 0, 1, 2, 3, 4)$ with $J^* = 1.0881887380 \times 10^{-2}$ kg-m^2 denoting the reference polar mass moment of inertia mentioned at the beginning of this section and the stiffness for each of the torsional springs is given $\hat{k}_{t,i} = k_t^*/5$ with $k_t^* = 6.891150988 \times 10^3$ Nm/rad denoting the reference stiffness. From Figure 8, one sees that the entire PN-taper shaft is composed of four shaft segments and the length of each shaft segment is given by $\Delta L_i = L_{\text{shaft}}/p = [(L_\ell + \overline{L}_\ell) - (L_s + \overline{L}_s)]/4 = [(5 + 5) - (3 + 3)]/4 = 1.0$ m. Since the concentrated elements are located at the ends of the shaft segments, their coordinates with respect to the origin o of the positive-taper shaft $\overline{AB}$ are given by $x_0 = 3.0$ m, $x_1 = 4.0$ m, $x_2 = 5.0$ m, $x_3 = 6.0$ m, and $x_4 = 7.0$ m, respectively, as one may see from Figures 8(a)–8(c).

For convenience of comparison, the lowest four natural frequencies and the five mode shapes of the "bare" free-free PN-taper shaft (without carrying any concentrated elements) are shown in the final row of Table 5 (denoted by bold-faced digits) and Figure 9(a), respectively. Comparing Table 5 for the current free-free PN-taper shaft with Table 4 for the free-free P-taper shaft, one sees that the conclusions drawn from Table 4 are also correct for Table 5. However, there exists a significant difference between Figures 9(b) and 7(b) that the lowest five mode shapes (including the quasi rigid-body mode) of the loaded PN-taper shaft shown in Figure 9(b) are symmetrical (or antisymmetrical) with

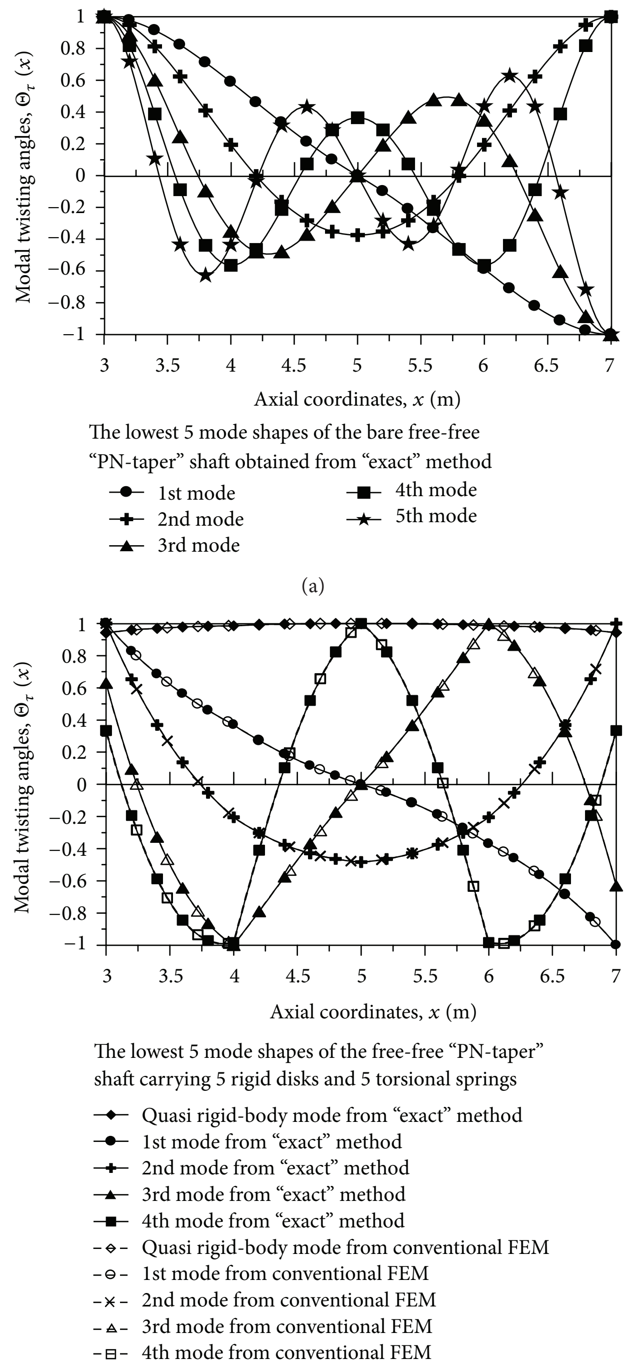

Figure 9: The lowest five mode shapes of the free-free PN-taper shaft with taper ratio $\overline{\alpha} = 0.01$ (cf. case 2 of Table 1): (a) for the bare shaft (without any attachment, cf. Figure 3); (b) for the loaded shaft (carrying 5 rigid disks and 5 torsional springs as shown in Figure 8).

respect to its middle cross-section due to the fact that both the structural dimensions and the loading conditions are symmetrical with respect to its middle cross-section, but this is not true for those of the loaded P-taper shaft shown in Figure 7(b). Of course, the lowest five mode shapes of the bare PN-taper shaft as shown in Figure 9(a) are also symmetrical (or antisymmetrical) with respect to its middle cross-section due to symmetry of the structure. The legends of Figure 9 are the same as those of Figure 7. It is seen that all mode shapes obtained from FEM are very close to the corresponding ones obtained from the exact method as one may see from Figure 9(b). This is under expectation because the associated natural frequencies shown in Table 5 are very close to each other.

9. Conclusions

(1) Since the exact solution for free torsional vibrations of the general conic shafts is not yet obtainable from the existing literature, the presented exact method is significant in this aspect. Besides, the exact natural frequencies and associated mode shapes for free torsional vibrations of the general conic shafts carrying any number of rigid disks or/and torsional springs obtained from the presented exact method are also significant for evaluating the accuracy of various existing approximate methods concerned (such as FEM).

(2) For a conic shaft composed of two shaft segments with opposite tapers, it is difficult to obtain its exact natural frequencies and associated mode shapes of free torsional vibrations. The simple theory presented in this paper is helpful for solving this kind of problem.

(3) The formulation of this paper is very flexible because (i) the locations of the concentrated elements on the shaft are arbitrary; (ii) the total number of concentrated elements attached to the shaft is also arbitrary including zero; and (iii) each node may be attached by a rigid disk or a torsional spring or both a rigid disk and a torsional spring.

(4) For a P-taper conic shaft with its (right) larger-end diameter d_ℓ and total length L kept constant (cf. Figure 5), its lowest five natural frequencies (ω_τ, $\tau = 1$ to 5) in the F-F, C-C, or F-C BCs decrease with the decrease of its taper ratio $\overline{\alpha}$ because the polar mass moment of inertia of the entire shaft increases with the decrease of $\overline{\alpha}$ and the influence of $\overline{\alpha}$ on the supporting stiffness is much smaller. The last trend is also true for the 2nd to 4th natural frequencies (ω_2 to ω_4) of the shaft with C-F BCs, but the 1st natural frequency (ω_1) increases significantly with the decrease of taper ratio $\overline{\alpha}$ because near the (left) clamped end, the increasing effect of supporting stiffness is much greater than that of polar mass moment of inertia due to the decrease of taper ratio $\overline{\alpha}$.

(5) For a conic shaft (either P-taper or PN-taper) carrying arbitrary rigid disks and the same number of torsional springs, if the locations of the rigid disks are identical to the corresponding torsional springs, then the lowest five natural frequencies of the shaft decrease due to carrying the rigid disks only and increase due to carrying the torsional springs only. However, the lowest five natural frequencies of the shaft carrying both the rigid disks and the torsional springs have the next relationship: $\omega_{i,J} < \omega_{i,Jk_t} < \omega_{i,k_t}$, where $\omega_{i,J}$, ω_{i,k_t}, and ω_{i,Jk_t} represent the ith natural frequencies of the conic shaft carrying the rigid disks only, the torsional springs only, and both the rigid disks and the torsional springs, respectively.

(6) For a conic shaft (either P-taper or PN-taper) carrying torsional springs or both rigid disks and torsional springs, there exists a quasi rigid-body natural frequency ω_0. The latter is slightly higher than the true rigid-body natural frequency defined by $\overline{\omega}_0 = \sqrt{\sum \hat{k}_{t,i}/(J_{\text{shaft}} + \sum \hat{J}_i)}$, where J_{shaft} denotes the polar mass moment of inertia of the entire shaft itself, while $\sum \hat{k}_{t,i}$ and $\sum \hat{J}_i$ denote the summation of stiffness of all torsional springs and that of polar mass moment of inertia of all rigid disks attached to the shaft, respectively.

Appendix

Exact Natural Frequencies and Mode Shapes of a Uniform Shaft

The characteristic equation for free torsional vibration of a uniform shaft is given by [7]

$$\Theta''(x) + \beta^2 \Theta(x) = 0, \tag{A.1}$$

where

$$\beta^2 = \frac{\omega^2 \rho}{G}. \tag{A.2}$$

The last expressions are similar to those of the same uniform shaft performing free longitudinal vibration [7]; thus, the exact solution for natural frequencies and mode shapes of free longitudinal vibration of a uniform shaft is available for those of free torsional vibration of the same shaft, if the Young's modulus E for longitudinal vibrations is replaced by the shear modulus G for torsional vibrations. The results for various boundary conditions are listed in the following.

(i) *F-F Shaft and C-C Shaft.* The exact natural frequencies for the torsional vibrations of a uniform shaft with free-free (F-F) boundary conditions are the same as those with clamped-clamped (C-C) ones. They are given by

$$\beta_\tau = \frac{\tau\pi}{L} \quad (\tau = 0, 1, 2, 3, \ldots, \infty),$$
$$\omega_\tau = \frac{\beta_\tau L}{L}\sqrt{\frac{G}{\rho}} = \frac{\tau\pi}{L}\sqrt{\frac{G}{\rho}} \quad (\tau = 0, 1, 2, 3, \ldots, \infty). \tag{A.3}$$

However, the associated mode shapes are different from each other and given by

$$\Theta_\tau(x) = A_\tau \cos\left(\frac{\tau\pi x}{L}\right) \quad (\tau = 0, 1, 2, 3, \ldots, \infty) \quad (\text{for F-F shaft}), \tag{A.4}$$

$$\Theta_\tau(x) = A_\tau \sin\left(\frac{\tau\pi x}{L}\right) \quad (\tau = 1, 2, 3, \ldots, \infty) \quad (\text{for C-C shaft}). \tag{A.5}$$

Since $\tau = 0$ represents the rigid-body mode, the formulas given by (A.3) with $\tau = 0$ are correct only for the F-F shaft.

(ii) *C-F Shaft*. The exact natural frequencies and mode shapes of a uniform shaft with clamped-free (C-F) boundary conditions are given by

$$\beta_\tau = \frac{\tau\pi}{2L} \quad (\tau = 1, 3, 5, \ldots, \infty), \tag{A.6}$$

$$\begin{gathered} \omega_\tau = \frac{\beta_\tau L}{L}\sqrt{\frac{G}{\rho}} = \frac{\tau\pi}{2L}\sqrt{\frac{G}{\rho}} \quad (\tau = 1, 3, 5, \ldots, \infty) \longrightarrow \\ \omega_s = \frac{(2s-1)\pi}{2L}\sqrt{\frac{G}{\rho}} \quad (s = 1, 2, 3, \ldots, \infty), \end{gathered} \tag{A.7}$$

$$\begin{gathered} \Theta_\tau(x) = A_\tau \sin\left(\frac{\tau\pi x}{2L}\right) \quad (\tau = 1, 3, 5, \ldots, \infty) \longrightarrow \\ \Theta_s(x) = A_s \sin\left(\frac{(2s-1)\pi x}{2L}\right) \quad (s = 1, 2, 3, \ldots). \end{gathered} \tag{A.8}$$

(iii) *F-C Shaft*. The exact natural frequencies and mode shapes for a uniform shaft with free-clamped (F-C) boundary conditions are given by

$$\beta_\tau = \frac{\tau\pi}{2L} \quad (\tau = 1, 3, 5, \ldots, \infty), \tag{A.9}$$

$$\begin{gathered} \omega_\tau = \frac{\beta_\tau L}{L}\sqrt{\frac{G}{\rho}} = \frac{\tau\pi}{2L}\sqrt{\frac{G}{\rho}} \quad (\tau = 1, 3, 5, \ldots, \infty) \longrightarrow \\ \omega_s = \frac{(2s-1)\pi}{2L}\sqrt{\frac{G}{\rho}} \quad (s = 1, 2, 3, \ldots), \end{gathered} \tag{A.10}$$

$$\begin{gathered} \Theta_\tau(x) = A_\tau \cos\left(\frac{\tau\pi x}{2L}\right) \quad (\tau = 1, 3, 5, \ldots, \infty) \longrightarrow \\ \Theta_s(x) = A_s \cos\left(\frac{(2s-1)\pi x}{2L}\right) \quad (s = 1, 2, 3, \ldots). \end{gathered} \tag{A.11}$$

It is noted that the frequency parameters β_τ given by (A.9) are the same as those given by (A.6), but the corresponding mode shapes $\Theta_\tau(x)$ defined by (A.11) are different from those defined by (A.8).

Acknowledgment

This work was supported by the National Science Council, the Republic of China, under Contract no. NSC 101-2221-E-022-002.

References

[1] J. S. Wu and C. T. Chen, "An exact solution for the natural frequencies and mode shapes of an immersed elastically restrained wedge beam carrying an eccentric tip mass with mass moment of inertia," *Journal of Sound and Vibration*, vol. 286, no. 3, pp. 549–568, 2005.

[2] S. Abrate, "Vibration of non-uniform rods and beams," *Journal of Sound and Vibration*, vol. 185, no. 4, pp. 703–716, 1995.

[3] B. M. Kumar and R. I. Sujith, "Exact solutions for the longitudinal vibration of non-uniform rods," *Journal of Sound and Vibration*, vol. 207, no. 5, pp. 721–729, 1997.

[4] Q. S. Li, "Torsional vibration of multi-step non-uniform rods with various concentrated elements," *Journal of Sound and Vibration*, vol. 260, no. 4, pp. 637–651, 2003.

[5] Y. Z. Chen, "Torsional free vibration of a cylinder with varying cross-section and adhesive masses," *Journal of Sound and Vibration*, vol. 241, no. 3, pp. 503–512, 2001.

[6] F. D. Faires and R. L. Burden, *Numerical Methods*, PWS, Boston, Mass, USA, 1993.

[7] L. Meirovitch, *Analytical Methods in Vibrations*, Macmillan, London, UK, 1967.

[8] C. R. Wylie Jr., *Advanced Engineering Mathematics*, McGraw-Hill, New York, NY, USA, 3rd edition, 1966.

[9] T. V. Karman and M. A. Biot, *Mathematical Methods in Engineering*, McGraw-Hill, 1940.

[10] G. N. Watson, *A Treatise on the Theory of Bessel Functions*, Cambridge University Press, 1952.

[11] H. B. Dwight, *Tables of Integrals and Other Mathematical Data*, Massachusetts Institute of Technology, 3rd edition, 1957.

[12] J. S. Przemieniecki, *Theory of Matrix Structural Analysis*, McGraw-Hill, New York, NY, USA, 1968.

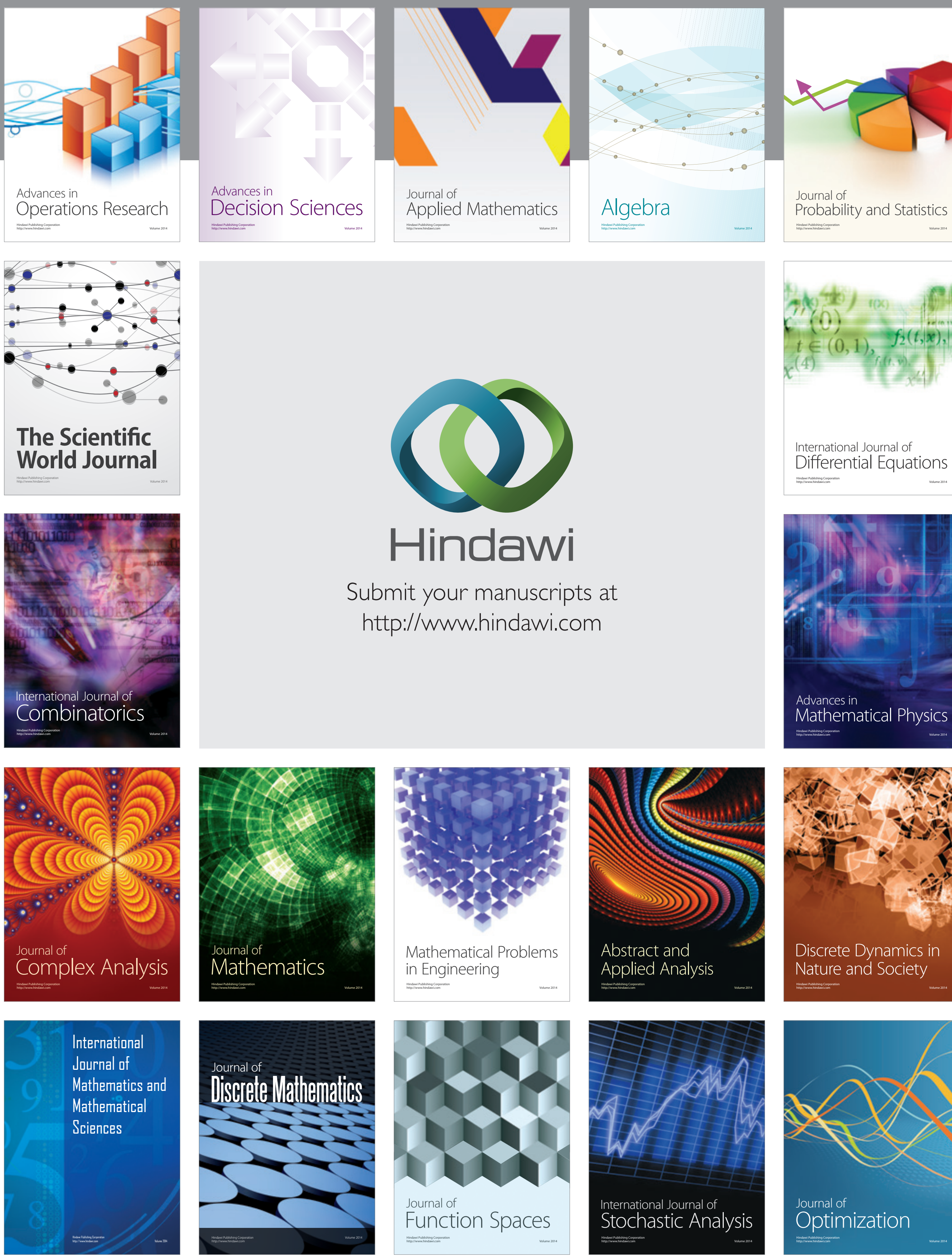

Advances in
Operations Research
Advances in
Decision Sciences
Journal of
Applied Mathematics
Algebra
Journal of
Probability and Statistics
The Scientific
World Journal
International Journal of
Differential Equations
Hindawi
Submit your manuscripts at
http://www.hindawi.com
International Journal of
Combinatorics
Advances in
Mathematical Physics
Journal of
Complex Analysis
Journal of
Mathematics
Mathematical Problems
in Engineering
Abstract and
Applied Analysis
Discrete Dynamics in
Nature and Society
International
Journal of
Mathematics and
Mathematical
Sciences
Journal of
Discrete Mathematics
Journal of
Function Spaces
International Journal of
Stochastic Analysis
Journal of
Optimization